

Review

Recent Advances in High-Temperature Properties of High-Entropy Alloys

Weiming Pan^{1,2}, Daoyuan Huang^{1,2}, Wanlin Wang^{1,2}, Guangyang Dou³ and Peisheng Lyu^{1,2,*}

¹ School of Metallurgy and Environment, Central South University, Changsha 410083, China; 223507003@csu.edu.cn (W.P.); hdy_aoe@163.com (D.H.); 213506005@csu.edu.cn (W.W.)

² National Center for International Research of Clean Metallurgy, Central South University, Changsha 410083, China

³ Jingxi City Daxinan Manganese Industry Co., Ltd., Jingxi 533800, China; 813289568@qq.com (G.D.)

* Corresponding author. E-mail: lyu.peisheng@csu.edu.cn (P.L.)

Received: 10 March 2025; Accepted: 4 June 2025; Available online: 11 June 2025

ABSTRACT: High-temperature alloys are critical for advanced thermal components in aerospace and energy industries. Conventional alloys, which rely on a single principal element with limited alloying additions, often exhibit insufficient phase stability and rapid oxidation at extreme temperatures. In recent years, high-entropy alloys (HEAs) have emerged as revolutionary candidates for high-temperature applications, overcoming the limitations of conventional alloys through their unique multi-principal element design and exceptional performance. This review systematically examines the latest progress in HEAs' key high-temperature properties: tensile properties, creep resistance, oxidation resistance, and phase stability. Research demonstrates that HEAs achieve remarkable mechanical properties at elevated temperatures through multiple mechanisms, such as lattice distortion effects, precipitation of ordered L1₂-structured phases, and refined grain boundary engineering. For instance, refractory HEAs like MoNbTaVW and Hf-Nb-Ti-V systems exhibit superior creep resistance at temperatures exceeding 1600 °C, outperforming traditional nickel-based superalloys. The slow diffusion of oxygen and the formation of multi-component oxide layers enhance the high-temperature oxidation resistance of high-entropy alloys. Additionally, HEAs display excellent phase stability under thermal exposure, driven by high configurational entropy and optimized microstructural designs, including nanoscale lamellar phases and coherent precipitates. Despite these advances, challenges remain in balancing mechanical strength with ductility, ensuring long-term durability under cyclic thermal-mechanical loads, and tailoring compositions for extreme service conditions. Future efforts should integrate machine learning, computational modeling, and high-throughput experiments to accelerate the discovery of novel HEA systems and validate their performance in practical applications. By addressing these challenges, HEAs are poised to revolutionize material solutions for next-generation aerospace engines, nuclear reactors, and high-efficiency energy systems.

Keywords: High-entropy alloys; High-temperature tensile properties; Creep resistance; Oxidation resistance; Phase stability



© 2025 The authors. This is an open access article under the Creative Commons Attribution 4.0 International License (<https://creativecommons.org/licenses/by/4.0/>).

1. Introduction

High-temperature metallic materials are vital in many industries [1,2], including aerospace, power generation and nuclear industries. However, throughout human history, traditional alloy design has typically relied on a single metal as the primary constituent [3], with only minor additions of alloying elements to achieve the required performance for practical applications. However, these alloys face limitations such as γ' -phase coarsening, oxide layer spallation above 1000 °C, and rapid degradation near their melting points. The traditional alloy design, ranging from early bronzes to modern steels [4], magnesium alloys [5], and aluminum alloys [6], is based on conventional phase diagram thermodynamics. It aims to restrict the number of constituent elements to prevent the formation of complex microstructures that could lead to processing difficulties or detrimental effects on mechanical properties. Traditional high-temperature alloys are no exception. For instance, nickel-based high-temperature alloys [7] are formulated with a Ni matrix alloyed with elements such as Cr and Mo; cobalt-based alloys [8] use Co with additions of Cr and W; and a series of cost-effective iron-based high-temperature alloys [9] have also been developed. Among these, nickel-based alloys are renowned for their excellent high-temperature strength and are widely employed in turbine blades of aero-

engines and combustion chambers of gas turbines [10]. At 800 °C, their specific strength even exceeds that of titanium alloys, while their composite Cr₂O₃/Al₂O₃ oxide films limit the oxidation rate to less than 0.1 mm/year (at temperatures below 1000 °C). Their high-temperature yield strength is effectively enhanced by two key mechanisms [11]: the lattice distortion effect resulting from the substitution of Ni with larger atoms (e.g., W, Mo, and Re) and the precipitation of a coherent, ordered L1₂-structured Ni₃(Al,Ti) (γ' phase) from the γ matrix. These alloys can typically operate within a temperature range of 650–1000 °C. Unfortunately, the γ' phase is prone to coarsening at elevated temperatures, and the strength of nickel-based single-crystal alloys deteriorates sharply when operating near 80% of their melting temperature (approximately 1100 °C). In addition, the protective Cr₂O₃ and Al₂O₃ oxide films tend to spall at temperatures above 1000 °C. In recent years, rapid advancements in high-temperature applications, especially in aerospace, have substantially increased the demand for high-temperature components with superior mechanical properties and oxidation resistance. For example, structural components are now expected to operate beyond 1200 °C under complex stress states and chemically aggressive environments. These evolving service demands far exceed the capabilities of current Ni- and Co-based systems, creating an urgent need for novel materials with ultrahigh temperature strength, oxidation resistance, and microstructural stability [12].

In response to these challenges, high entropy alloys (HEAs) have attracted extensive attention [13] due to their high melting points at elevated temperatures, excellent phase stability, and superior mechanical properties. Some HEAs show promise for high-temperature applications and may potentially replace nickel-based superalloys as next-generation high-temperature materials [14]. HEAs represent a novel class of alloys formed by combining multiple metallic elements in equiatomic or near-equiatomic proportions [15,16]. They exhibit phenomena such as the high-entropy effect, sluggish diffusion effect, lattice distortion effect, and cocktail effect [17], which overcome the limitations of conventional alloys that rely on a single principal element. This innovative approach greatly expands the compositional design space and has sparked a new materials revolution, fostering the integration of machine learning, computational simulations, and high-throughput screening techniques in materials science [18]. Since the concept of high entropy alloys was first introduced in 2004 [19], these alloys have garnered significant interest worldwide for their unique phase structures and optimal mechanical properties [3,15,20–23]. Extensive experimental research by scholars around the globe has further uncovered the potential of HEAs in high-temperature environments.

Based on their compositional characteristics and structural features, they can be mainly categorized into the following types:

- (1) Refractory HEAs (RHEAs) are composed primarily of elements such as Nb, Mo, Ta, and W, exhibiting ultra-high melting points and excellent high-temperature strength and creep resistance, making them suitable for aerospace propulsion and nuclear applications.
- (2) Eutectic HEAs (EHEAs) are characterized by a dual-phase structure (FCC + B2 or FCC + L1₂), which provides a balance between strength and ductility, good castability, and thermal stability, making them ideal for high-temperature structural components.
- (3) Al-containing HEAs benefit from the addition of Al to promote ordered B2 or L1₂ phases, significantly improving high-temperature mechanical strength and oxidation resistance; they are commonly used in thermal barrier coatings and protective surface layers.
- (4) Oxidation-resistant HEAs such as AlCrMoTaTi can form dense and stable oxide films (Al₂O₃, Cr₂O₃) at elevated temperatures, offering excellent oxidation protection up to 1300 °C.
- (5) Lightweight HEAs incorporate low-density elements like Al, Ti, Mg, or Li, offering high specific strength while reducing overall weight, making them suitable for aerospace structural applications.

These diverse types of HEAs, through multi-component alloying and microstructural design, demonstrate substantial potential for future high-temperature applications.

In addition, some studies have demonstrated the potential application of HEA films produced by advanced manufacturing methods, such as PVD technology, in extreme mechanical and thermal environments. Alvi [24] et al. developed a nanocrystalline CuMoTaWV HEA film using direct current magnetron sputtering with a target prepared via spark plasma sintering (SPS) of equimolar elemental powders. The resulting film, exhibiting a body-centered cubic (BCC) solid solution structure with a preferred (110) orientation, achieved a hardness of 19 GPa and a compressive strength of 10 GPa. The incorporation of copper not only contributed to enhanced plasticity but also facilitated the formation of a lubricating CuO oxide layer at elevated temperatures, thereby significantly improving wear resistance at 300 °C (with a wear rate 102 times lower than stainless steel). In a separate study [25], the same group synthesized an amorphous thin-film metallic glass (TFMG) composed of eight refractory elements (HfMoNbTaTiVWZr) and further

derived nitride variants by reactive sputtering with controlled nitrogen flow ratios. These nitride films demonstrated remarkable thermal stability (up to 950 °C) and superior mechanical performance, including hardness values reaching 18.7 GPa and compressive strengths over 10 GPa. Moreover, the as-deposited metallic glass showed exceptional ductility (~60% strain without fracture), highlighting the role of high configurational entropy, lattice distortion, and strong interatomic bonding in enhancing high-temperature mechanical reliability. These findings underscore the versatility of sputtered HEA films in structural applications where simultaneous strength, thermal stability, and wear resistance are required.

This review presents a comprehensive overview of recent advances in the high-temperature mechanical properties, oxidation resistance, and phase stability of HEAs and provides perspectives on future developments in high-temperature HEAs research. It aims to offer valuable insights and guidance for the design and development of next-generation HEAs optimized for extreme service environments.

2. High-Temperature Mechanical Properties

2.1. Tensile Strength and Ductility

High-temperature short-term mechanical properties [26] refer to the yield strength and elongation exhibited by a material during short-term testing at elevated temperatures. As one of the key indicators of alloys' high-temperature performance, strength and ductility are particularly critical for applications operating at moderate temperatures or for components subjected to very short service durations [27], such as those in rockets and missiles [28]. Generally, as the temperature increases, the yield strength of metallic materials decreases while their ductility increases.

Figure 1 illustrates the variation in specific strength and yield strength of several alloy materials with temperature. It can be observed that HEAs exhibit remarkable strength retention at elevated temperatures. As shown in Figure 1, the AlCoCrFeNi alloy achieves a specific strength of 200 MPa·cm³/g within the temperature range of 800–900 °C, surpassing that of TiAl alloys at comparable temperatures. Furthermore, the VNbMoTaW alloy retains a specific strength of approximately 70 MPa·cm³/g even at 1500 °C. High-entropy alloys HEAs exhibit exceptional mechanical properties across a wide temperature spectrum from 0 to 1600 °C [29]. For instance, the MoNbTaVW HEA maintains a yield strength of 300–500 MPa at 1600 °C, whereas the yield strength of Inconel 718 drops sharply from ~1000 MPa at 500 °C to <200 MPa at 800 °C. These results highlight the superior mechanical performance of some HEAs in high-temperature environments compared to traditional alloy systems.

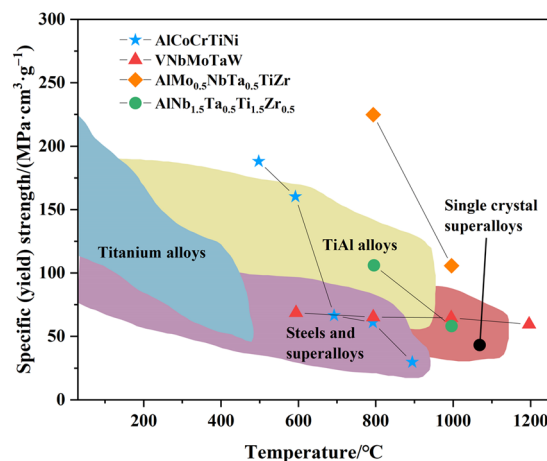


Figure 1. High-temperature specific strength of the HEAs compared with other materials [30].

In recent years, significant progress has been made in enhancing the high-temperature mechanical properties of HEAs. The core advantage of HEAs stems from their unique multi-principal element design, which enables synergistic strengthening mechanisms such as solid-solution strengthening, precipitation phase control, and grain boundary optimization [31]. These multiscale interactions effectively balance high-temperature strength and ductility in HEAs.

Among these, solid-solution strengthening plays a foundational role, as the severe lattice distortions induced by multi-principal element mixing hinder dislocation motion and enhance strength across a broad temperature range. Alloys such as AlMo_{0.5}NbTa_{0.5}TiZr and AlNbTaTiZr [32] exemplify this approach, where the substitution of elements like Mo with Ta further improves oxidation resistance by promoting the formation of dense, adherent oxide films without compromising mechanical properties. In addition, as demonstrated in CoCrFeNiW_{0.2} HEA [33], the

incorporation of refractory W leads to pronounced solid-solution strengthening effects by impeding dislocation mobility and contributing to dynamic strain aging, as evidenced by the evolution of serrated flow behavior (A→B→C) under increasing temperature. Complementing this, precipitation strengthening is widely employed to enhance both strength and thermal stability. In systems like $\text{Al}_1\text{Ti}_5\text{Zr}_4\text{Nb}_3\text{Ta}_3$ and $\text{AlNbTi}_3\text{VZr}_{1.5}$ [34,35], the formation of nanoscale B2 and HCP precipitates provides strong barriers to dislocation glide and enables sustained work hardening during plastic deformation, even at elevated temperatures. These finely dispersed secondary phases are thermally stable and uniformly distributed, thus effectively delaying softening and maintaining load-bearing capacity under service conditions. Similarly, the $\text{Al}_{0.3}\text{CoCrFeNi}$ alloy exhibits nanoscale B2 precipitates enriched in Al and Ni, which interact with dislocations and deformation twins, thereby influencing strain-hardening behavior across 300–700 °C. Notably, these precipitates form preferentially along grain boundaries, stabilizing microstructure against coarsening [36]. Interfacial strengthening is another pivotal mechanism that significantly contributes to the mechanical robustness of these alloys. Alloys such as $\text{TiNbTaWC}_{0.7}$ and NbMoTaWHf [37,38] incorporate coherent or semi-coherent phase boundaries, often with specific orientation relationships like $\{111\}\text{FCC} // \{110\}\text{BCC}$ or faceted zig-zag interfaces that increase the resistance to dislocation penetration and enhance high-temperature structural integrity. These interfaces act as effective obstacles to deformation and play a crucial role in grain boundary stabilization. Moreover, transformation-induced strengthening mechanisms further expand the design space for achieving superior mechanical behavior. In the case of $\text{AlCoCrFeTi}_{0.5}\text{Ni}_{2.5}$ [35], the synergistic interplay between deformation-induced twinning in the FCC matrix and stress-assisted martensitic transformation in the BCC phase leads to enhanced strain hardening and delayed necking, resulting in both high strength and improved ductility at elevated temperatures.

A novel, low-effective L_{12} -strengthened single-crystal HEA ($\text{Co}_{37.8}\text{Ni}_{38.6}\text{Cr}_{5.2}\text{Mo}_{5.1}\text{Al}_{9.8}\text{Ta}_{2.6}\text{Ti}_{3.9}$) was successfully developed through directional solidification. [39] The high-entropy alloy with this composition was fabricated using directional solidification. As illustrated in Figure 2, after heat treatment, the L_{12} phase was uniformly distributed within the FCC matrix, with an average size of approximately 280 nm. These precipitates exhibited a highly coherent interface with the matrix (lattice mismatch of only 0.14%) and a volume fraction as high as 80%, which exceeds that of conventional single-crystal superalloys. [40,41]. Moreover, no detrimental topologically close-packed (TCP) phases were observed. At an intermediate temperature of 800 °C, the alloy exhibited a maximum yield strength of 897 MPa, an ultimate tensile strength of 1038 MPa, and an elongation of 37%. Moreover, at elevated temperatures (900 °C and 1000 °C), the HEA maintained excellent performance.

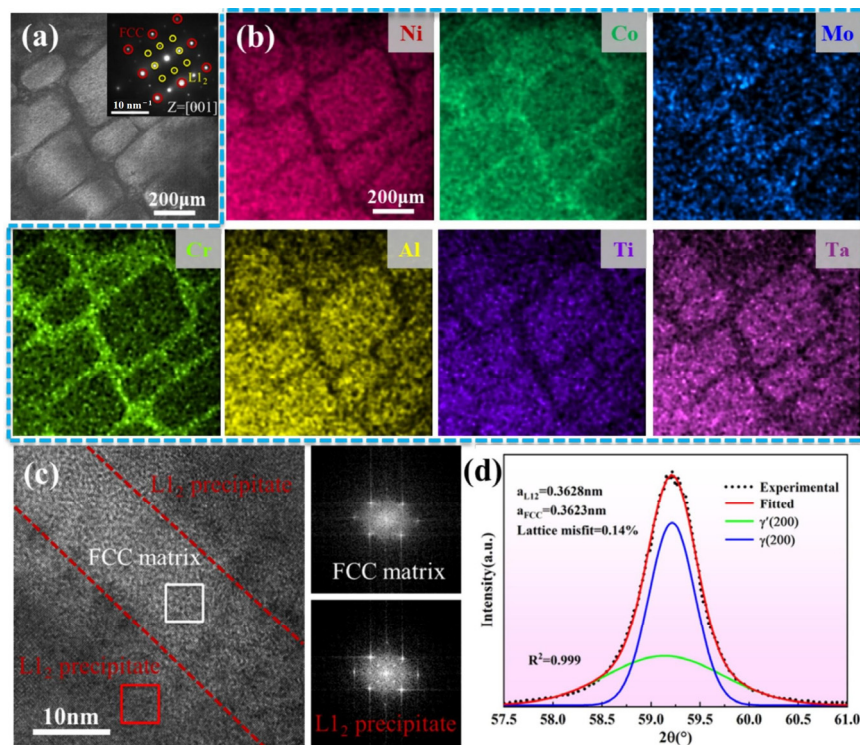


Figure 2. (a) Dark-field TEM image exhibiting the high-density L_{12} precipitates embedded in the matrix of $\text{Co}_{37.8}\text{Ni}_{38.6}\text{Cr}_{5.2}\text{Mo}_{5.1}\text{Al}_{9.8}\text{Ta}_{2.6}\text{Ti}_{3.9}$ alloy. (b) STEM-EDX elemental mapping of the sample, exhibiting the elemental distribution behavior. (c) HR-TEM image of the interface between the FCC matrix and L_{12} precipitates and their corresponding FFT patterns. (d) Deconvolution of the (200) diffraction peak of the alloy showing the lattice misfit between the precipitates and matrix [39].

Meanwhile, Lei Gao [42] et al. developed a novel Ni-Co-Cr-Al-based high-entropy superalloy (HESA) that exhibits outstanding high-temperature mechanical properties across a broad temperature range. This alloy features a face-centered cubic (fcc) matrix with low stacking fault energy (SFE). Their study demonstrated that the addition of Ti, Nb, Ta, Mo, and W to the Ni-Co-Cr-Al-based HESA effectively reduces the SFE of the fcc matrix and promotes the precipitation of nanoscale, near-spherical, multi-component particles with coherent interfaces (as shown in Figure 3). Remarkably, this HESA achieves an ultimate tensile strength (UTS) of ~ 1100 MPa at 750 °C, surpassing the performance of other contemporary materials.

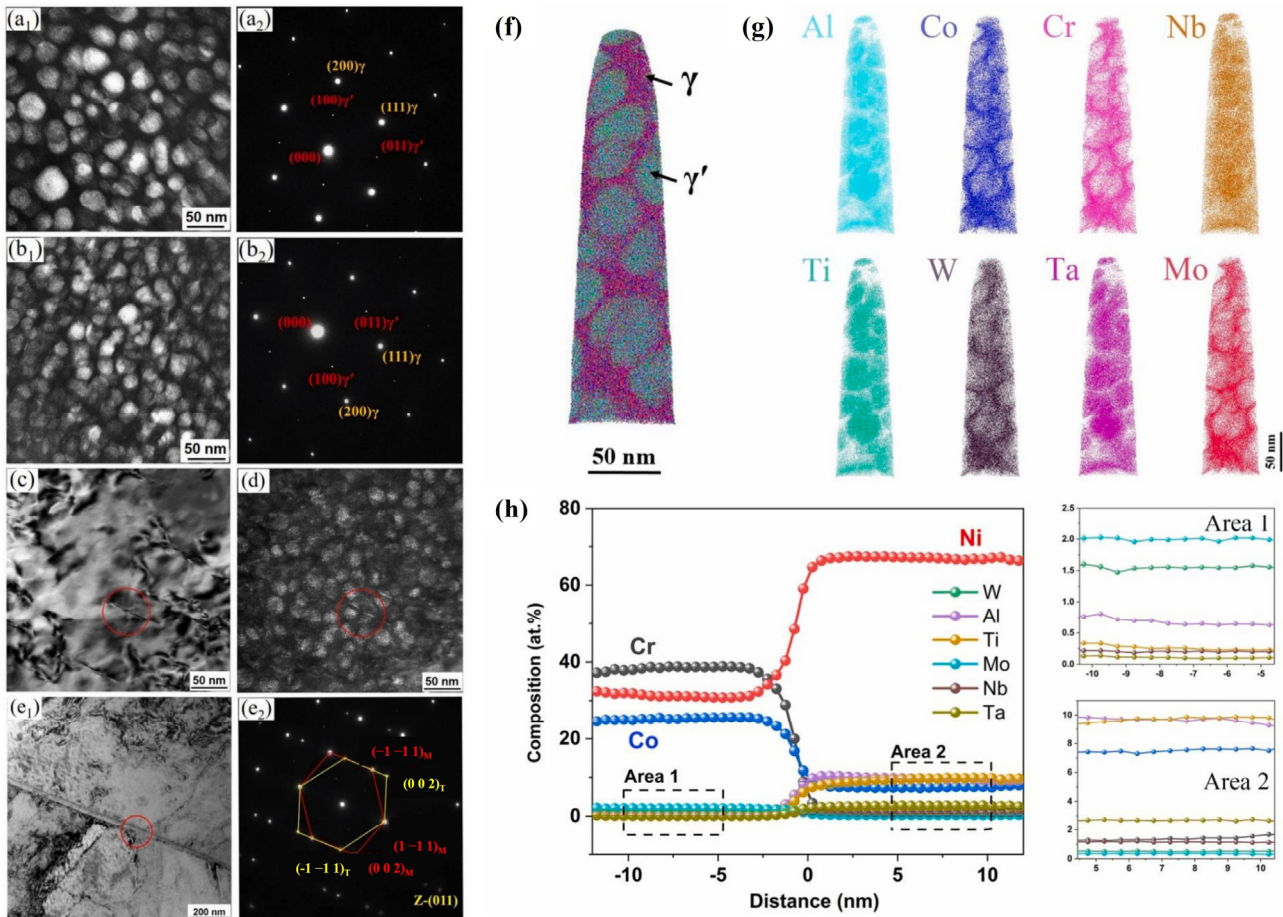


Figure 3. Dark field TEM images and SAED patterns of $(\text{Ni}_{50}\text{Co}_{20}\text{Cr}_{25}\text{Al}_{15})_{99.4-x}(\text{Mo}_{12.5}\text{W}_{12.5}\text{Ta}_{12.5}\text{Nb}_{12.5}\text{Ti}_{50})_x\text{Co}_{0.6}$, $x = 7.5$ (a1,a2) and $x = 10$ (b1,b2) respectively; Bright field (c) and dark field (d) images of γ' precipitates, and bright field image (e1) and SAED pattern (e2) of twin structure in $x = 7.5$ alloy. (f) Projected 3-D APT reconstruction with nanoparticles. (g) The atom maps of Al, Co, Cr, Nb, Ti, W, Ta and Mo elements. (h) Proximity histogram of concentration profiles across the γ matrix and γ' nanoparticles [42].

B.X. Cao [43] et al. developed an L_{12} -strengthened, multi-component Co-rich high-entropy alloy (HEA) with exceptional microstructural stability. Their study revealed that high-density cuboidal γ' precipitates were uniformly embedded within the alloy matrix. Remarkably, even after prolonged isothermal aging at 800 – 1100 °C, no brittle intermetallic phases formed at grain boundaries or within grains. As illustrated in Figure 4, atom probe tomography (APT) analysis demonstrated that Ta and Nb preferentially partitioned into the γ' intermetallic phase, which is critical for stabilizing the L_{12} -ordered crystal structure. Notably, this alloy exhibited an optimal combination of a high γ' solvus temperature (1125 °C), low mass density (8.28 g/cm³), and excellent high-temperature tensile strength (755 MPa at 800 °C and 664 MPa at 900 °C), surpassing the performance of other Co-based HEAs [44,45] and several conventional superalloys. These findings provide a valuable paradigm for designing advanced Co-based L_{12} -strengthened high-temperature alloys with extended operational temperature ranges.

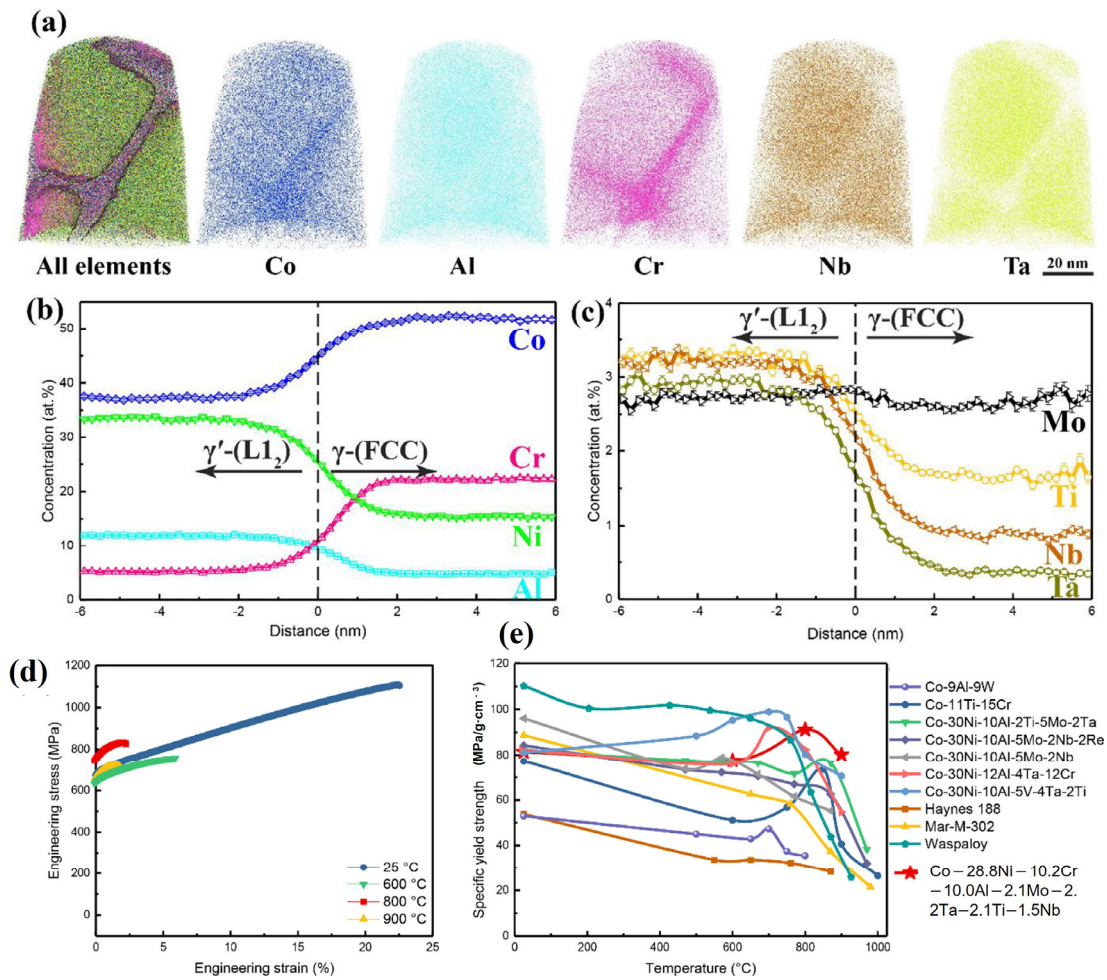


Figure 4. (a) Ion maps of different elements. 14 at.% Cr iso-concentration surface was used to illustrate the γ/γ' interfaces in the ion map, which contains all elements. (b,c) Proximity histograms of individual elements across the γ/γ' interfaces, showing distinctly different elemental compositions between the γ matrix and the γ' precipitates. (d) Engineering stress-strain curves of the MCoHEA at ambient and elevated temperatures. (e) The plots between specific yield strength and deformation temperature [43].

Chanho Lee [46] developed a refractory NbTaTiV high-entropy alloy (HEA) with a single body-centered cubic (BCC) structure using a combined experimental and theoretical approach. A typical dendritic microstructure was observed, which was attributed to elemental segregation during solidification in the as-cast state. However, after an appropriate homogenization treatment at 1200 °C for three days, structural inhomogeneity and chemical segregation were completely eliminated. Atomic probe tomography (APT) quantitatively confirmed the uniform distribution of elements. Importantly, the results demonstrated that this HEA exhibits both high yield strength and ductility at room temperature and elevated temperatures (up to 900 °C). Furthermore, first-principles calculations were conducted to analyze and quantify the effect of high configurational entropy on mechanical properties based on lattice distortion and atomic interactions within the NbTaTiV HEA. The study revealed that severe local lattice distortion is induced due to atomic interactions and atomic size mismatches in the homogenized NbTaTiV refractory HEA, significantly contributing to its superior mechanical performance.

An Hf–Nb–Ti–V refractory high-entropy alloy (RHEA) was successfully fabricated by Yongyun Zhang [47] using directed energy deposition (DED), exhibiting excellent tensile properties across a wide temperature range. This performance was primarily attributed to the introduction of severe lattice distortion in the as-fabricated RHEA, which resulted from localized chemical fluctuations and significant atomic radius mismatches. These factors, combined with strong solute pinning effects, contributed to the exceptional yield strength of the DED-manufactured RHEA across a broad temperature spectrum. This alloy design strategy, which involves introducing substantial lattice distortion while maintaining a low-temperature sensitivity of the elastic modulus, opens new possibilities for the direct fabrication of RHEAs with outstanding high-temperature performance.

Yuhao Jia [48] discovered that the addition of a small amount of boron significantly strengthens both FCC grain boundaries and FCC/B2 phase interfaces in the Ni₃₀Co₃₀Cr₁₀Fe₁₀Al₁₈W₂ eutectic high-entropy alloy (EHEA) at high temperatures. Even with a minor boron addition, the alloy achieved an impressive tensile yield strength exceeding 581

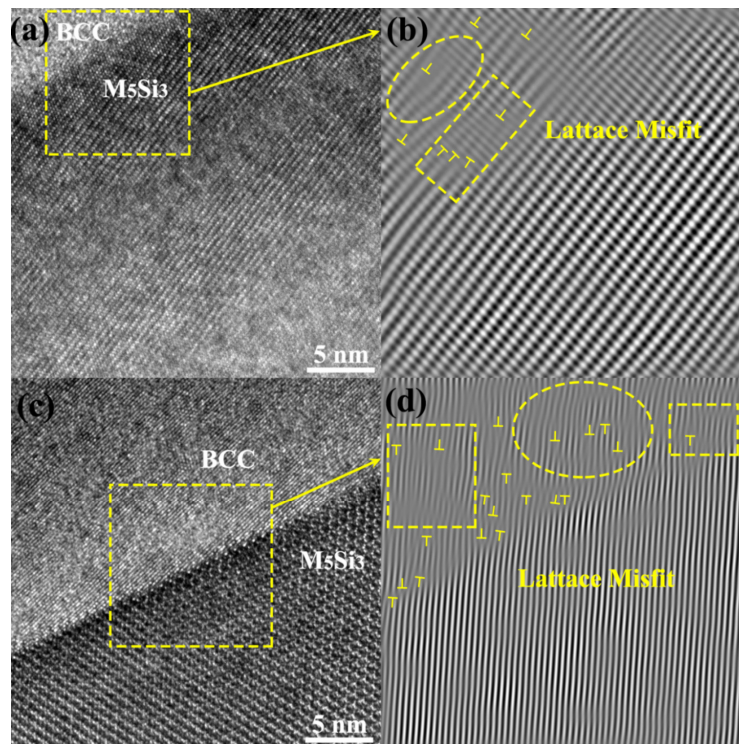


Figure 6. High-resolution transmission electron microscopy (HRTEM) images of $\text{AlMo}_{0.5}\text{NbTiVSi}_x$ alloy: (a) $\text{Si}_{0.2}$ alloy. (c) $\text{Si}_{0.5}$ alloy, Inversed Fast Fourier Transform (FFT) images: (b) $\text{Si}_{0.2}$ alloy. (d) $\text{Si}_{0.5}$ alloy [49].

2.2. Creep Resistance

High-temperature alloys often face cyclic loading in high-temperature environments, making their creep resistance crucial for engineering applications [53]. Creep [54] in metallic materials refers to the phenomenon where strain increases over time under constant stress. Unlike plastic deformation, creep occurs even when the stress is below the elastic limit. Therefore, evaluating the creep performance of new materials is vital for their practical engineering use. Over nearly two decades of development, HEAs have demonstrated numerous advantages in high-temperature environments, with growing attention being paid to their creep behavior [55].

Conventional high-temperature alloys, such as nickel-based alloys, improve creep resistance through the precipitation of strengthening phases, such as the γ' phase. This strengthening mechanism performs well at high temperatures; however, it has a limitation: as the temperature increases further, the precipitate phases may coarsen or dissolve, leading to a decline in performance. Additionally, traditional high-temperature alloys tend to experience grain boundary weakening at elevated temperatures, where segregation and uneven distribution of precipitates at the grain boundaries can reduce their strength, thus affecting the alloy's creep resistance. For HEAs, their slow element diffusion dynamics and lattice distortion effects effectively suppress dislocation motion and grain boundary sliding at high temperatures, theoretically improving their creep resistance. However, conventional high-temperature alloys still have competitive advantages in the medium-temperature range and mature application scenarios. At present, only some HEAs exhibit creep resistance superior to traditional high-temperature alloys, and the creep mechanisms of HEAs at high temperatures remain insufficiently understood [56]. However, some recent studies have also promoted the understanding of the creep behavior of high entropy alloys at high temperatures.

In non-equiatomic FeMnCoCrAl , asymmetric atomic arrangements enhance solute drag and dislocation climb mechanisms under sustained stress [57]. Molecular dynamics simulations reveal that increasing W content in NbMoTaW enhances solute drag and grain stability, improving creep resistance at the atomic level [58]. In $\text{AlTiVNbZr}_{0.25}$, Nb_2Al precipitates formed at B2 phase interfaces enhance dislocation pinning, resulting in class-A creep at 1073 K [59]. Similarly, single-crystal high-entropy superalloys (HESAs) utilize spherical γ' precipitates to retard dislocation movement via bypass and climb, ensuring resistance at intermediate temperatures [60]. LPBF-processed Ti-Ta-Nb-Mo-Zr RHEAs exhibit enhanced creep resistance via dislocation tangles and high-stress exponents under 923–1023 K [61]. In $\text{AlCoCrFeNi}_{2.1}$ EHEA, the dual-phase lamellar $\text{L}_{1/2}/\text{B}_2$ structure induces varied dislocation glide and shear behavior with temperature, resulting in temperature-dependent creep characteristics between 700–900 °C [62].

Te-Kang Tsao [63] introduced a novel high-entropy alloy and investigated its high-temperature tensile and creep behaviors. At 982 °C, its creep resistance is comparable to some nickel-based high-temperature alloys. Experimental results indicate that the alloy's matrix has low stacking fault energy, the strengthening precipitates possess high anti-phase boundary energy, and the microstructure is thermally stable, all contributing to the enhancement of HESA's properties. The creep curve of this HEA primarily exhibits three-stage creep behavior. The low creep rate of this high-entropy alloy is attributed to slow diffusion, low stacking fault energy in the γ matrix, and high creep activation energy.

M. Zhang [64] conducted tensile creep tests on the CrMnFeCoNi high-entropy alloy at temperatures ranging from 1023 K to 1173 K, as shown in Figure 7. The stress exponent was calculated using the following formula:

$$\dot{\varepsilon}_{ss} = A\sigma^n \exp\left(-\frac{Q_c}{RT}\right) \quad (1)$$

where $\dot{\varepsilon}_{ss}$ is steady-state creep rate, σ is applied stress, A is a material constant, n is the stress exponent, Q_c is the apparent activation energy of creep, R is the ideal gas constant, and T is the absolute temperature.

Their study revealed that the stress exponent for the CrMnFeCoNi high-entropy alloy remained consistent at 3.7 ± 0.1 across all tested temperatures. The apparent activation energy for creep was determined to be approximately 230 kJ/mol, which decreased with increasing applied stress, indicating stress-assisted thermally activated behavior. The steady-state creep microstructure was characterized by the absence of sub-grain formation within the grains and a high dislocation density. Based on their findings, the creep rate of CrMnFeCoNi was primarily controlled by dislocation-dislocation interactions and dislocation-lattice interactions. This suggests that the creep behavior at high temperatures is influenced by the dynamics of dislocations in the material's crystal structure.

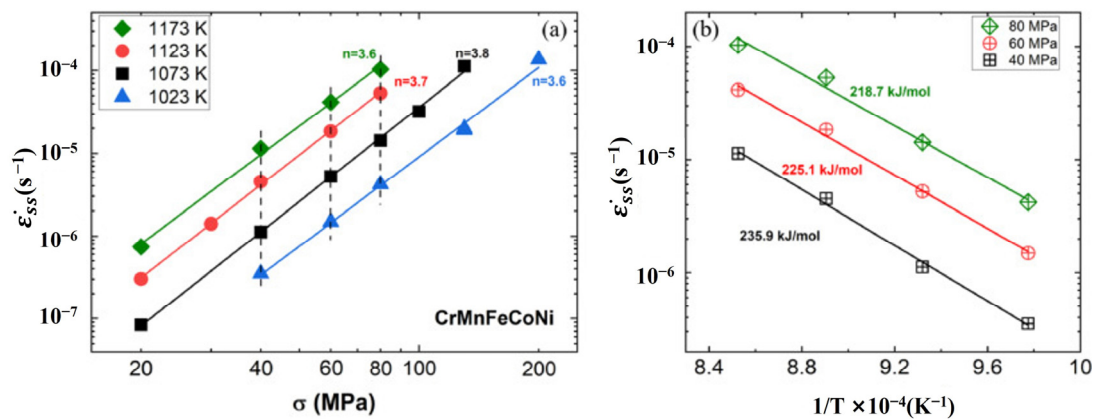


Figure 7. (a) Double logarithmic plot of steady-state creep rate versus applied stress for CrMnFeCoNi tested from 1023 K to 1173 K at 50 K intervals. (b) Arrhenius plot that shows the temperature dependence of steady-state creep rate at three isostresses of 80, 60, and 40 MPa. The calculated activation energies of creep are also labeled on the plot [64].

Xun Shen [56] prepared a bulk nanocrystalline VNbMoTaW refractory high-entropy alloy (RHEA) with an average grain size of 67 ± 17 nm via mechanical alloying (MA) followed by high-temperature, high-pressure sintering. Compression and creep tests were conducted to evaluate its high-temperature mechanical properties at 973 K and 1073 K. Although the creep performance of the nanocrystalline VNbMoTaW RHEA was slightly lower than that of its coarse-grained counterpart, it was significantly superior to previously reported coarse-grained and ultrafine-grained HEAs [59,65,66] (Figure 8e,f). Observations indicated that creep deformation was primarily controlled by grain boundary diffusion, particularly due to the slow diffusion rates of Mo and Nb, which dominate the high-temperature creep behavior. Moreover, STEM-EDS analyses (Figure 8a–d) revealed the segregation of V at the grain boundaries, further enhancing the alloy's thermal stability and creep resistance. This work provides a fundamental understanding of the creep behavior and deformation mechanisms in nanocrystalline RHEAs, which will aid in the design of advanced, creep-resistant materials.

Che-Jen Liu [67] et al. conducted a study on the creep deformation mechanisms of the high-entropy alloy HfNbTaTiZr, specifically below 1250 °C. They employed optical floating zone (OFZ) technology to prepare HfNbTaTiZr with an average grain size greater than 1 mm. The tensile creep tests were performed in a vacuum at temperatures ranging from 1100 °C to 1250 °C, under 5–30 MPa of progressively applied stress. The stress exponent and creep activation energy were determined to be 2.5–2.8 and 273 ± 15 kJ/mol, respectively. The experimental results are shown in Figure 9. The calculated stress exponent indicated a solute drag creep behavior, with the deformation

controlled by $a/2 \langle 111 \rangle$ dislocations. To further investigate the influence of alloy composition on solute drag creep, they also simulated the intrinsic diffusion coefficients of all elements and compared the theoretical minimum creep strain rate with experimental values. Their analysis showed that the creep rate of HfNbTaTiZr was likely controlled by Ta, which exhibited the lowest intrinsic diffusion rate, thus contributing the most to solute drag and controlling the resistance to dislocation motion.

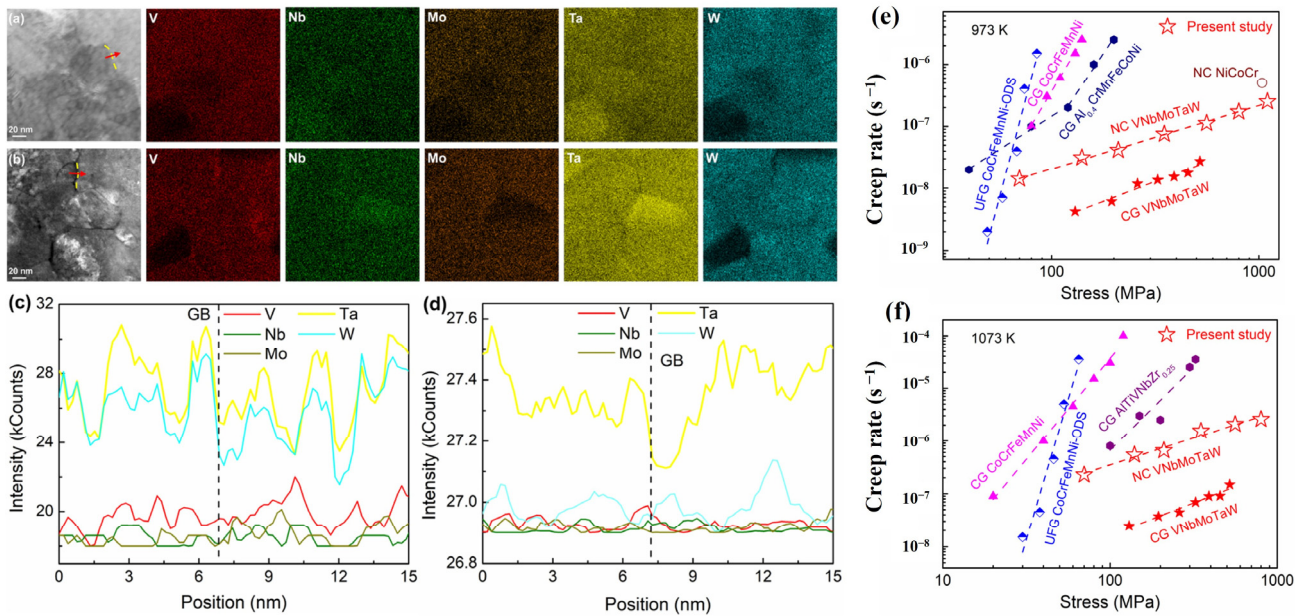


Figure 8. (a,b) STEM-HAADF image of the bulk NC VNbMoTaW and (c,d) the corresponding EDS elemental mappings. (a) As-sintered specimen. (b) Specimen after creep at 1073 K under a stress of 560 MPa. (c,d) Representing the corresponding EDS concentration profiles of V, Nb, Mo, Ta, and W measured from the EDS line scan performed along the red arrow shown in (a,b), respectively. Yellow dashed lines in (a,b) and vertical dashed lines in (c,d) represent the position of GB. Creep rate vs. stress for the bulk NC VNbMoTaW at (e) 973 K and (f) 1073 K in comparison with previously reported CG and UFG HEAs [56].

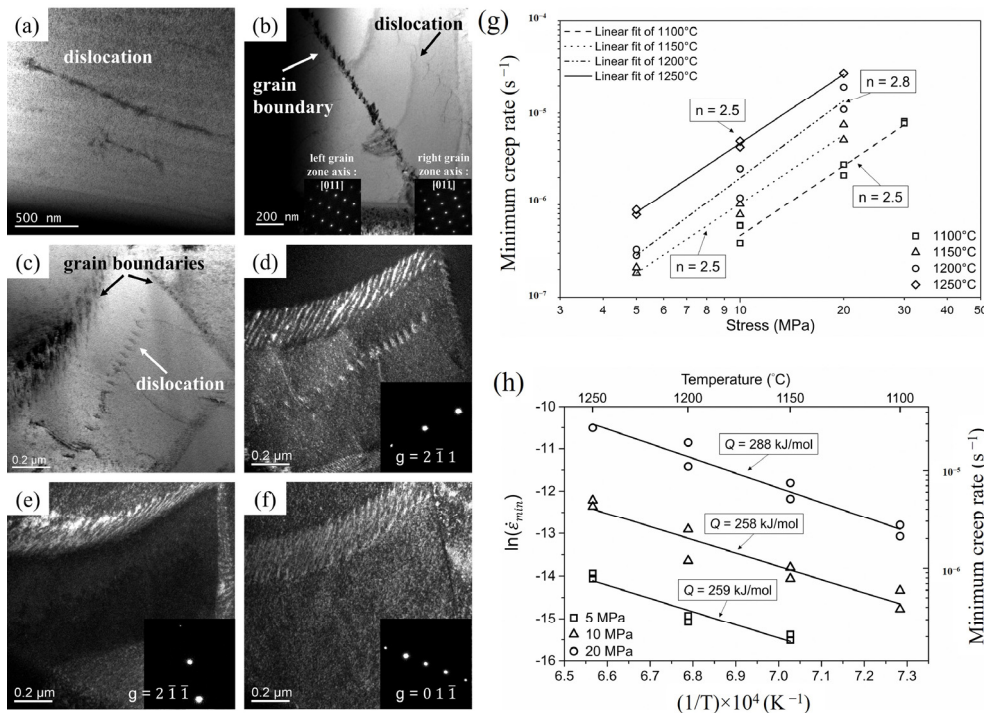


Figure 9. TEM images of HfNbTaTiZr after creep at 1100 °C. (a) dislocation structure within grain interior; (b,c) overview of dislocation and grain boundary structure after creep; (d–f) Weak-beam dark-field micrographs from the same area of (c) in zone axis near (d) $[11\bar{3}]$, (e) $[13\bar{1}]$ and (f) $[1\bar{1}\bar{1}]$. (g) Minimum creep rates versus applied stress from 1100 to 1250 °C. (h) minimum creep rates versus the reciprocal of the absolute temperatures from 5 to 20 MPa [67].

Liu Yang [68] et al. synthesized a 27.3Ta-27.3Mo-27.3Ti-8Cr-10Al high-entropy alloy (HEA) via arc melting and fabricated bulk materials using high-temperature high-pressure sintering. The alloy's creep behavior was evaluated through compression creep tests at 1000 °C under an applied stress of 125 MPa, revealing a minimum creep rate of $\sim 2.5 \times 10^{-9} \text{ s}^{-1}$ (Figure 10). Within the temperature range of 1000~1030 °C, the alloy demonstrated excellent creep resistance, primarily attributed to the precipitation strengthening effect of B2 phases and remarkable microstructural stability. At 1000 °C and 1030 °C, the B2 precipitates underwent directional coarsening, forming a raft-like structure akin to those observed in Ni-based superalloys. Notably, the creep resistance of this HEA was comparable to the single-crystal Ni-based superalloy CMSX-4 [69] and even surpassed it under specific conditions. These findings provide critical theoretical and experimental foundations for the development of novel high-temperature alloys.

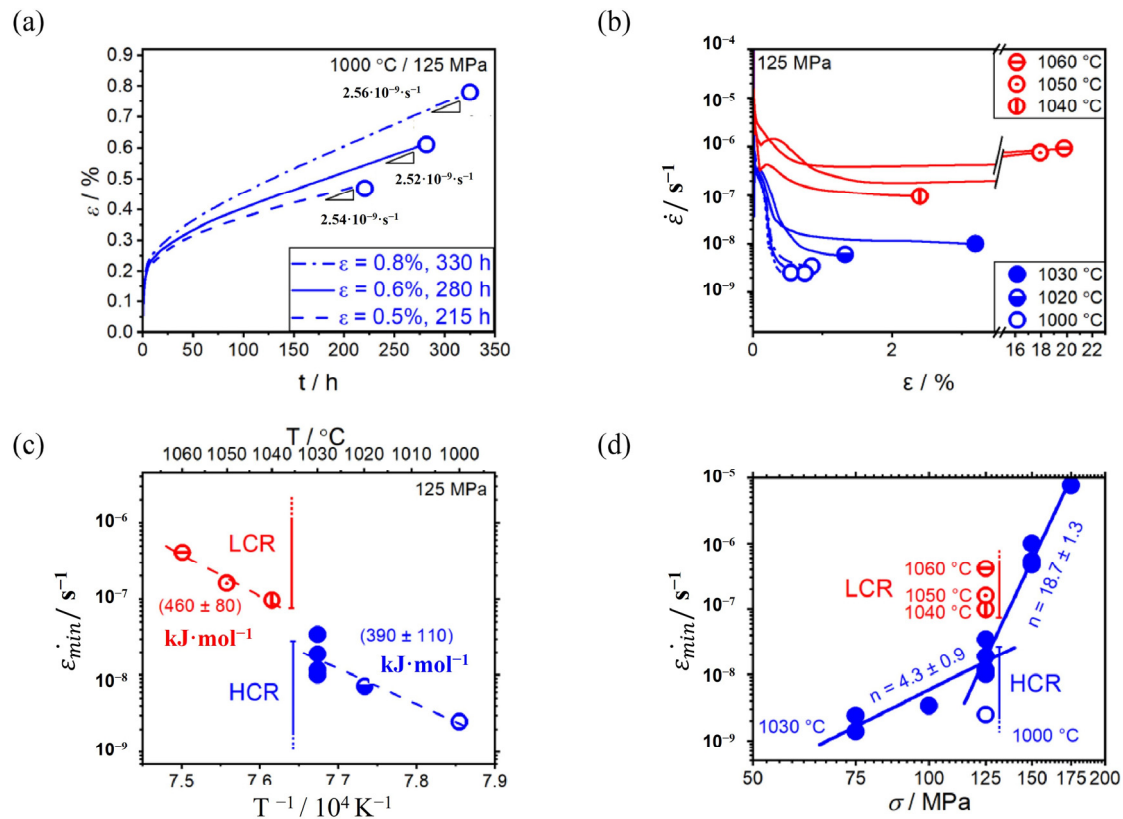


Figure 10. Creep behavior of TMT-8Cr-10Al. The creep regimes are demarcated as high creep resistance (HCR) marked in blue and low creep resistance (LCR) depicted in red: (a) creep strain ϵ as a function of time t for 125 MPa and 1000 °C. (b) Logarithmic plot of creep rate $\dot{\epsilon}$ vs. strain ϵ for 125 MPa at different temperatures. (c) Arrhenius plot for 125 MPa. HCR data corresponds to temperatures of 1000 °C, 1020 °C and 1030 °C, and LCR to 1040 °C, 1050 °C and 1060 °C. (d) Norton plot [68].

3. High-Temperature Oxidation Resistance

High-temperature oxidation resistance refers to a material's ability to resist oxidation reactions in high-temperature environments [70]. When materials are exposed to high-temperature oxidizing conditions, they chemically react with oxygen to form oxides. Materials with good high-temperature oxidation resistance can slow down the oxidation reaction rate [70], preventing rapid growth and peeling of the oxide layer, thereby maintaining the material's integrity and performance. HEAs can form protective multi-component oxide layers with slow oxygen diffusion and usually possess excellent high-temperature oxidation resistance.

Some alloying elements commonly found in traditional high-temperature alloys actually hinder improvements in oxidation resistance. For example, Vanadium (V) is easily oxidized. Moreover, V_2O_5 has a low melting point (690 °C) and a low boiling point (1750 °C), making it prone to melting or vaporizing at high temperatures [71]. Tungsten (W) exhibits intense evaporation of tungsten trioxide above 1150 °C, and the evaporation of the oxide can cause the oxide film to become porous, allowing oxygen to penetrate the metal-oxide interface, thus significantly increasing the oxidation rate. Additionally, niobium (Nb) alloys' oxides are not easily melted or vaporized at high temperatures, but the solubility and diffusion coefficient of oxygen are high [72]. Without protective coatings, the oxidation rate of conventional Nb alloys is very rapid, and their weight gain can be substantial, often exceeding 150 mg/cm² per hour.

The high-temperature oxidation resistance of HEAs is predominantly governed by the formation and stability of oxide scales, which are dictated by alloy composition and microstructural features. A widely effective mechanism involves the formation of dense and adherent protective oxides such as Al_2O_3 and Cr_2O_3 . Alloys like AlCrCoFeNi and $\text{FeCoNiCr}_{0.8}\text{Al}_{0.2}$ exhibit parabolic oxidation kinetics, with oxide layers composed mainly of Cr_2O_3 and Al_2O_3 , which act as effective diffusion barriers and maintain structural integrity during long-term exposure [73,74]. In some systems, complex multi-layered oxide scales are formed. For instance, CoCrCuFeNi and $\text{Cr}_x\text{MoNbTiV}$ develop outer spinel oxides, intermediate layers like NiFe_2O_4 or $\text{Ti}_4\text{Cr}_3\text{Nb}_3\text{O}_2$, and inner Cr_2O_3 or TiO_2 -rich layers, creating a graded structure that impedes oxygen penetration [75,76].

Furthermore, the addition of reactive elements such as Si and Hf significantly affects oxidation behavior. Si promotes the formation of continuous, slow-growing SiO_2 or Cr_3Si oxides in systems like CrFeNiTiSi and $\text{MoNbVTa}_{0.5}\text{Si}_{0.5}$, thereby enhancing oxidation resistance at intermediate temperatures [77,78]. Conversely, excessive Hf may introduce mismatch stresses, leading to oxide scale spallation, as observed in $\text{TaMoNbCrAl}_{0.5}\text{Hf}_{0.5}$ [79]. Microstructural control is also critical: in dual-phase or nanostructured HEAs (e.g., $\text{AlCoCr}_{0.5}\text{Fe}_{2.5}\text{Ni}_{2.5}$, AlFeCrMnTi), coherent precipitates and reduced grain boundary diffusion enhance the formation of stable oxides, while poorly designed interfaces may accelerate oxidation [80,81]. Additionally, the sluggish diffusion effect inherent to HEAs contributes to oxidation resistance, as observed in AlCrCoFeNi where HT-XRD reveals the dynamic evolution of protective oxide films under vacuum, and in $(\text{TiZrTa})_{50}\text{Ni}_{25}\text{Co}_{10}\text{Cu}_{15}$, where stable Ti-Ta-rich oxides inhibit spallation even at 1000 °C [73,82].

Compared to traditional high-temperature alloys, some refractory HEAs exhibit significantly improved oxidation resistance [83], and many scholars have conducted extensive studies on their mechanisms. First, in refractory HEAs, composite oxides can form. For example, in the NbTiZrV high-entropy alloy, TiNb_2O_7 and $\text{Nb}_2\text{Zr}_6\text{O}_{17}$ are formed, and in $\text{NbCrMo}_{0.5}\text{Ta}_{0.5}\text{TiZr}$ alloy, $\text{Nb}_3\text{Cr}_2\text{O}_{10}$ and $\text{Nb}_2\text{Zr}_8\text{O}_{21}$ are formed. In TaMoCrTiAl alloys, CrTaO_4 is formed [71,72,83]. As a result, during the oxidation process, the solubility of oxygen in refractory HEAs is lower compared to conventional refractory alloys. Secondly, due to the high alloying and high-entropy effects, oxygen diffusion in refractory HEAs is very slow. In the $\text{NbCrMo}_{0.5}\text{Ta}_{0.5}\text{TiZr}$ alloy, at 1000 °C, the effective oxygen diffusion coefficient through the oxide/alloy is approximately $3.0 \times 10^{-9} \text{ cm}^2/\text{s}$, which is two orders of magnitude lower than the oxygen diffusion in pure Nb [84]. Thirdly, because refractory often have high contents of Cr and Al, this favors the formation of protective oxides, such as Cr_2O_3 and Al_2O_3 , on the surface of refractory HEAs. As a result, their oxidation rates are reduced.

Jinpeng Zhang [85] studied the initial oxidation behavior of the AlCrMoNbTi HEA using a combination of experiments and density functional theory (DFT) calculation. The results indicated that oxygen atoms tend to occupy adsorption sites containing Ti atoms. Therefore, Ti atoms are more likely to combine with oxygen atoms, leading to the formation of compounds that hinder the formation of protective oxides such as Al_2O_3 and Cr_2O_3 . The calculations also showed that Cr atoms can form stable Cr-O bonds in a Ti-rich environment, which can enhance oxidation resistance by modifying the Cr-rich oxide layer. The short-term oxidation of AlCrMoNbTi HEA is illustrated as follows. In the initial stage of oxidation, as shown in Figure 11b, a sandwich-like oxide layer was identified, predominantly composed of a Ti-rich layer, with Al and Cr oxides dispersed within it. A surface oxide layer forms on the alloy sample, and as the oxidation deepens, the following oxide layers sequentially form beneath the Ti-rich layer: $(\text{TiCrNb})\text{O}_2$, $\alpha\text{-Al}_2\text{O}_3$, and $\alpha\text{-Cr}_2\text{O}_3$ (Figure 11c,d).

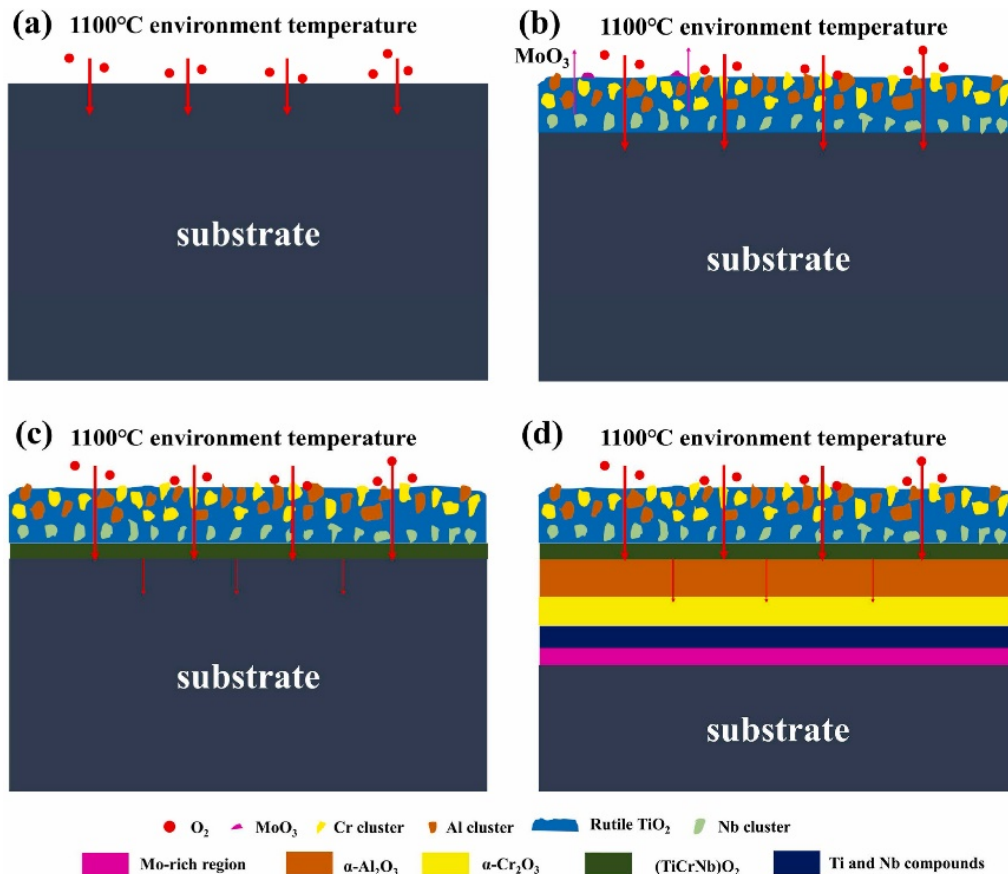


Figure 11. Diagrams of the oxidation mechanism of the AlCrMoNbTi HEA at 1100 °C [85].

Mengtian Liang [86] also investigated the effect of Ti content on the oxidation behavior of AlCoCrNiTi_x HEAs at 900 °C. The results indicated that optimal Ti doping reduced the oxidation rate by two orders of magnitude and promoted the formation of protective α -Al₂O₃, demonstrating the critical role of Ti in stabilizing the oxide scale and preventing spallation. These findings provide a theoretical basis for designing AlCoCrNi-based HEAs with improved high-temperature performance. Figure 12a–e show the surface morphologies of the Ti0, Ti0.1, Ti0.4, Ti0.7, and Ti1.0 samples after 2 h of oxidation at 900 °C. The Ti0 sample exhibited noticeably irregular oxidation, resulting in an incomplete oxide film with many pores. In contrast, the oxides formed on the Ti0.1, Ti0.4, Ti0.7, and Ti1.0 samples were well developed, consisting primarily of Al₂O₃ with an increased presence of Cr₂O₃.

Zhe Li [87] utilized electron beam freeform fabrication (EBF³) to refine the microstructure of refractory and enhance their oxidation resistance. High-temperature cyclic and isothermal oxidation tests were conducted at 1000 °C. Compared to the as-cast state, the remelted and deposited samples showed a reduction of 17.49% and 30.46%, respectively (Figure 13a,b), in total weight gain after 60 h of cyclic oxidation. The oxidation kinetics indicated that the treated samples had significantly lower mass gain and oxidation rates, demonstrating superior high-temperature oxidation resistance (Figure 13c) compared to others [88–92]. This improvement was attributed to the significant grain refinement achieved through the EBF³ process. The refined grain structure helps enhance the oxidation resistance of the alloy because smaller grains reduce defects at the grain boundaries, thereby decreasing the oxygen diffusion rate. Moreover, the samples formed a multi-layer oxide scale, including TiO₂, Al₂O₃, SiO₂, and AlNbO₄. This multi-layer structure effectively hinders further oxygen diffusion, thereby improving the alloy's oxidation resistance.

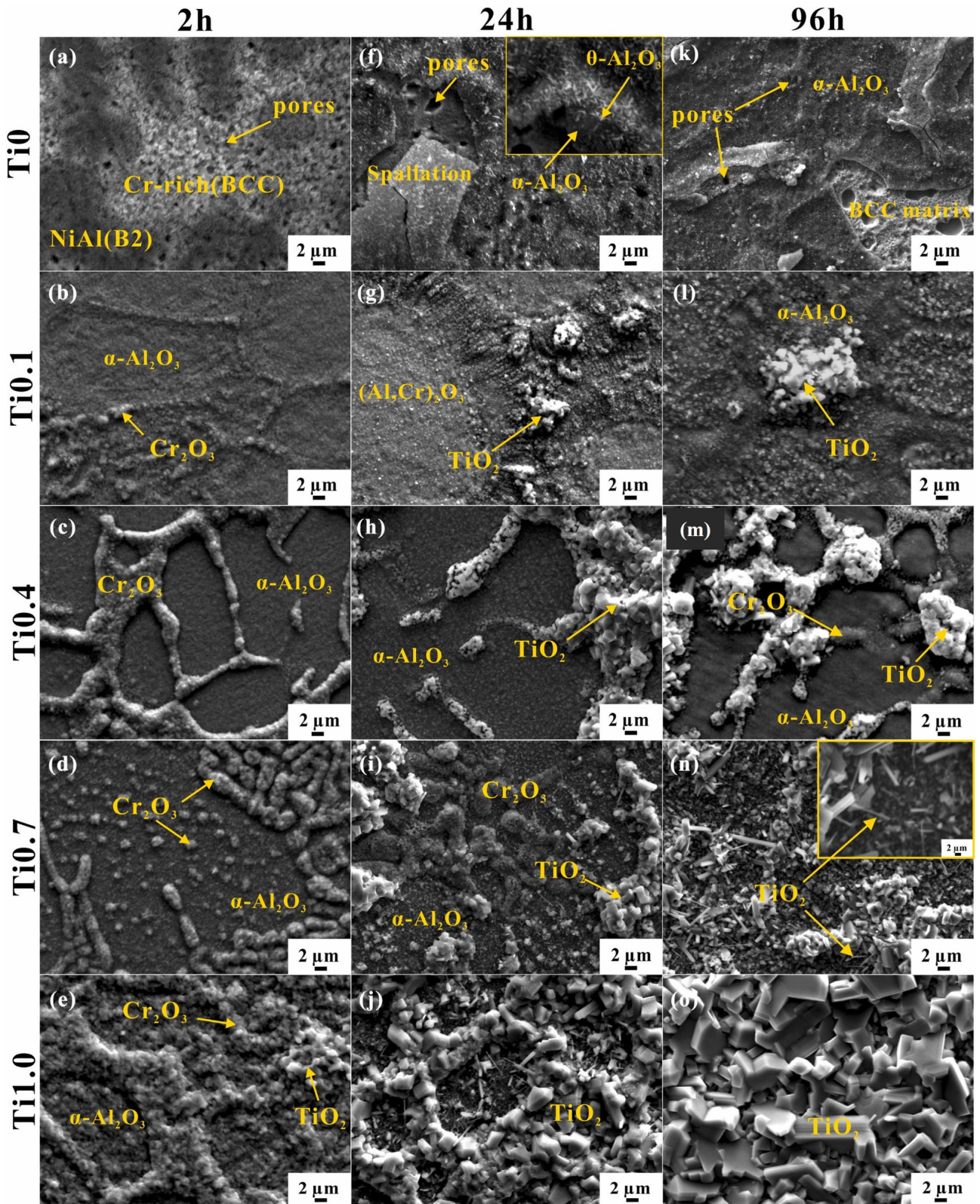


Figure 12. SEM images of the surface oxide layer of five HEAs after oxidation at 900 °C for: (a–e) 2 h, (f–j) 24 h, (k–o) 96 h [86].

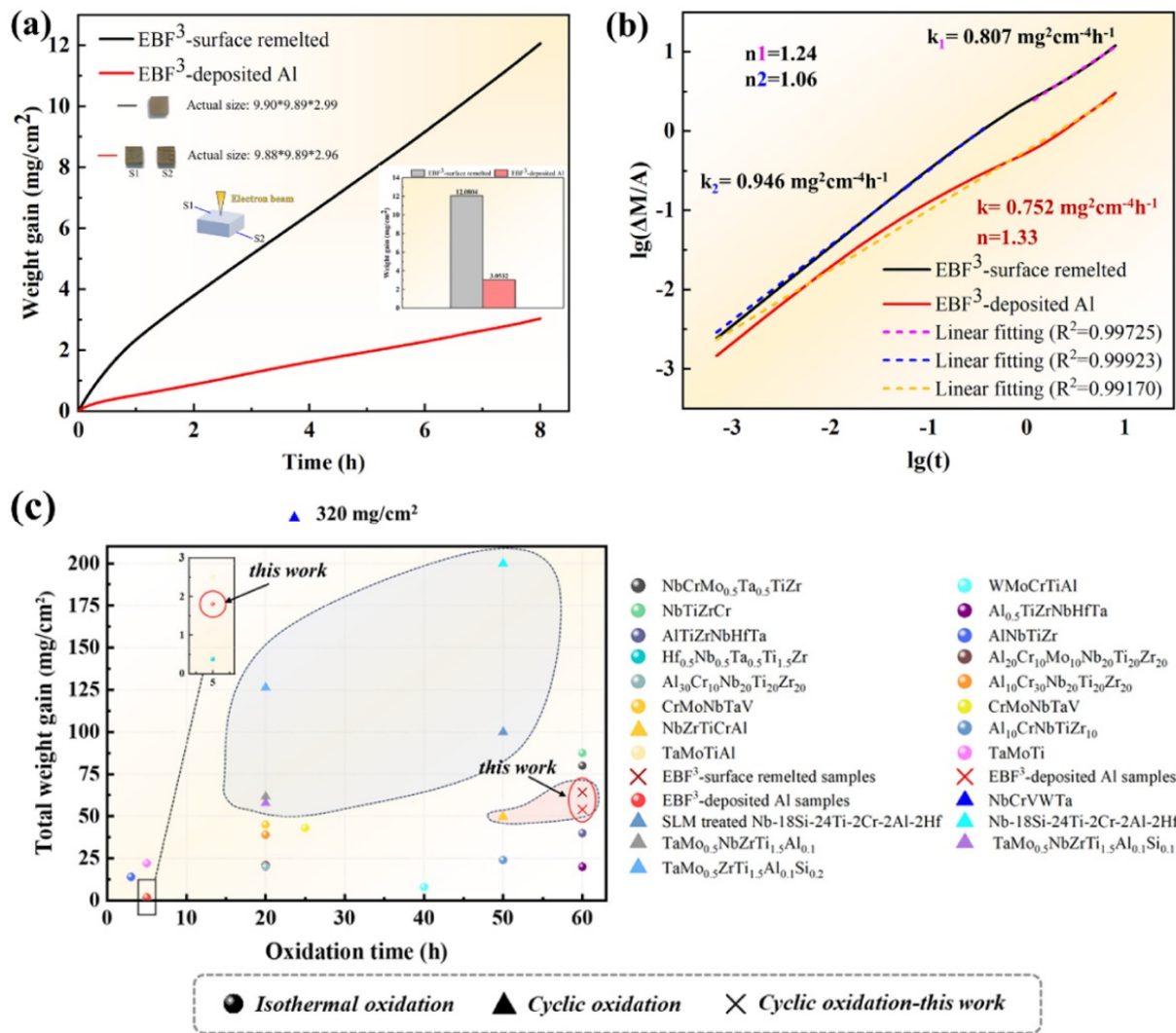


Figure 13. Isothermal oxidation kinetics of the two treated alloys (EBF³ remelted and EBF³ Al-deposited) at 1000 °C for 8 h (the experiments were conducted in TAG with 10 °C/min argon heating and static lab air oxidation). (a) Pure oxidation stage. Here, the macroscopic oxidation surface and original dimensions were embedded in the diagram. Sides S1 and S2 show the variability in macroscopic morphology. (b) lg(ΔM/A)–lg(t) plot, the k values here represent only the slope. (c) Oxidation properties comparison with other RHEAs and Nb-Si based alloys, *i.e.*, total weight gain versus oxidation time under 1000 °C [87].

Ling Li [93] developed a new Y-Hf co-doped NiCoCrAlPt high-entropy alloy (HEA) and investigated its long-term oxidation behavior at 1200 °C. The alloy exhibited a two-phase eutectic microstructure consisting of a γ' matrix and β' martensitic precipitates. The results showed that the alloy demonstrated excellent oxidation resistance by forming a unique, slowly growing Al₂O₃ oxide scale, which remained intact after 1000 h of oxidation at 1200 °C. This outstanding performance is attributed to the fine microstructure, increased Y/Hf solubility, low oxide growth stress, and the Pt-rich Al oxide/metal interface free from S segregation. These findings provide scientific insights for the design of Pt-containing oxidation-resistant.

Mingyi Guo [94] studied the oxidation behavior of MoNbVTa_{0.5}Cr_x (x = 0.25–1) refractory (RHEA) at 800 °C. The oxidation resistance of the alloy significantly increased with the increase in Cr content. Due to the formation of a dense CrNbO₄/CrTaO₄ oxide layer, the MoNbVTa_{0.5}Cr alloy exhibited good oxidation resistance. After 36 h of oxidation in air at 1100 °C, the mass gain was 47.76 mg/cm². The oxidation kinetics of the alloy between 800 °C and 1100 °C followed parabolic kinetics, with internal oxidation primarily caused by inward diffusion of oxygen. This study provides valuable references for the development of oxidation-resistant RHEAs.

From the oxidation mass gain curves of MoNbVTa_{0.5}Cr_x alloys (Figure 14a), the mass gain per unit area after 1 h of oxidation at 800 °C gradually decreased with increasing Cr content, indicating enhanced oxidation resistance. The XRD patterns of the MoNbVTa_{0.5}Cr_x refractory high-entropy alloys (RHEAs) after 1-h oxidation at 800 °C are shown in Figure 14b. The primary oxidation products of these alloys include Nb₂O₅, Ta₂O₅, CrTaO₄, and CrNbO₄. As the Cr content increased, the diffraction peak intensities of Nb₂O₅ and Ta₂O₅ progressively weakened, while those of CrTaO₄ and CrNbO₄ intensified. Furthermore, the presence of the BCC phase was detected on the surface of the Cr-containing

alloys, suggesting that the oxide layer formed was relatively thin. Notably, MoO_3 and V_2O_5 phases were absent in the XRD patterns of the oxidized samples. This absence is attributed to the low melting points of MoO_3 (795 °C) and V_2O_5 (690 °C), which render them highly volatile at temperatures above 800 °C, consistent with prior studies [95].

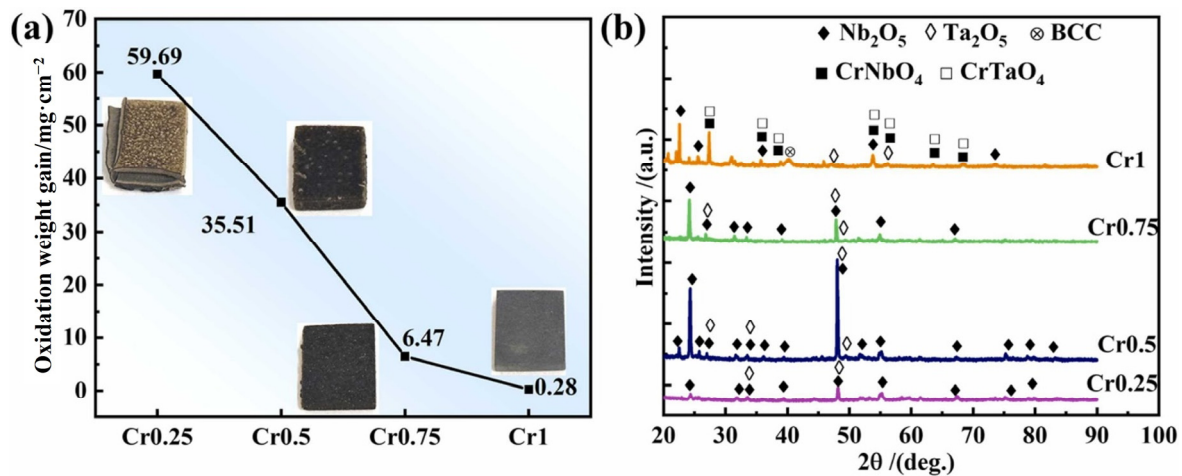


Figure 14. MoNbVTa_{0.5}Cr_x RHEAs oxidized at 800 °C for 1 h: (a) oxidation weight gain. (b) XRD pattern after oxidation [94].

4. High-Temperature Phase Stability

The microstructure plays a crucial role in determining the properties of alloys, yet alloys typically experience microstructural coarsening at high temperatures, which severely impacts their performance. Phase stability refers to the ability of these alloys to maintain their microstructure and phase composition under high-temperature conditions, including the matrix phase and precipitate phases. This stability is essential for the application of alloy materials in high-temperature environments, especially in fields such as aerospace, energy, and chemicals. Exhibit better phase stability [96,97] at high temperatures compared to conventional high-temperature alloys, mainly due to their slow diffusion characteristics and entropy-driven stabilization. In addition, researchers have proposed diverse mechanisms to improve the phase stability of high entropy alloys under extreme conditions, including grain boundary pinning and microstructural refinement, precipitation strengthening, phase transformation control, compositional suppression of deleterious phases, and advanced microstructure engineering.

Sikdar et al. [98] synthesized a nanocrystalline $(\text{AlCoCrCuFeNi})_{99}\text{B}_1$ alloy via mechanical alloying and spark plasma sintering, where boron segregation at interfaces effectively inhibited grain growth and phase decomposition. As a result, the grain size remained ultrafine (~76 nm) after 10 h of annealing at 1173 K, with only ~3% reduction in hardness, demonstrating superior structural and phase stability. Precipitation strengthening was exemplified by Shah [99] et al., who designed a eutectic $\text{CoCrFeNiTa}_{0.395}$ alloy that formed L1_2 and Ni_3Ta precipitates during deformation, thereby stabilizing the FCC matrix and resisted coarsening at temperatures beyond 0.8 T_c . Similarly, Liu [100] et al. developed a Fe-Ni-based HEA containing coherent γ/γ' precipitates with minimal coarsening (~40 nm after 1000 h at 1023 K), resulting in excellent creep resistance (61.5 h at 973 K under 450 MPa). In terms of phase transformation mechanisms, Sharma [101] et al. observed a B2-to-omega (hP18) transformation in Al-containing refractory HEAs at 800 °C, indicating that B2 is metastable and susceptible to structural reordering via element redistribution. Complementarily, Fan [102] et al. demonstrated that the apparent B2 phase in Al-Nb-Ta-Ti-Zr HEAs is often a quenched-in, non-equilibrium structure that lacks thermodynamic stability above 700 °C. From the compositional control perspective, Yi [103] et al. successfully suppressed σ phase formation between 860 and 1200 °C in AlCoCrFeNiTi alloys by adjusting Al/Ni/Cr ratios, resulting in excellent oxidation resistance and spallation resistance (>770 h at 1100 °C). Conversely, Whitfield [104] et al. showed that long-term annealing (1000 h) of AlMoNbTaTiZr alloys induced Al-Zr-rich hexagonal and orthorhombic precipitates, highlighting stability degradation despite initially ordered microstructures. Microstructure engineering has also proven effective: Mugale [105] et al. tuned the Al/Ni atomic ratio in AlCuFeNiTi systems to achieve stable FCC + BCC dual-phase microstructures, which maintained ductility (22.9%) and minimal strength loss after 24 h annealing at 900 °C. Chen [106] et al. designed $\text{Ti}_{30}\text{V}_{30}\text{Cr}_5\text{Zr}_5\text{Ta}_{15}\text{W}_{15}$ HEAs with excellent high-temperature strength (558 MPa at 1000 °C) and superior radiation resistance, surpassing pure tungsten instability. Additionally, Sun [107] et al. employed laser powder bed fusion (LPBF) to fabricate CoCrNiFeMn HEAs with dislocation cell structures and columnar grains, showing negligible

recrystallization or hardness degradation even after prolonged exposure to 1373 K. Together, these studies illustrate that enhancing high-temperature phase stability in HEAs requires a multi-mechanism strategy involving chemical design, thermodynamic control, and structural tailoring. These findings offer a robust foundation for engineering HEAs capable of long-term service in extreme thermal environments.

Hasan Kotan [108] et al. synthesized Sm-doped nanocrystalline CoCrFeNi via mechanical alloying and subsequently subjected it to annealing at temperatures up to 1100 °C for durations extending to 24 h. Microstructural observations at different processing stages (as shown in Figure 15) revealed significant grain coarsening in the CoCrFeNi alloy during annealing, with grain sizes reaching $\sim 1.35 \pm 0.5 \mu\text{m}$ after 1 h at 1100 °C ($T/T_m = 0.74$). This indicates that the nanocrystalline microstructure of CoCrFeNi lacks thermal stability under high-temperature conditions. In contrast, Sm-doped samples maintained an average grain size of 110 nm after 1 h of annealing at 1100 °C, demonstrating significantly enhanced thermal stability. This resistance to grain growth was attributed to the presence of rare-earth Sm and the formation of Sm/Cr-O mixed oxide phases at grain boundaries. Their findings highlight the potential to optimize the high-temperature thermal stability of CoCrFeNi HEAs for diverse applications.

Bang Xiao [109] used vacuum induction melting to produce the cast WMoTaNb refractory high-entropy alloy (RHEA), which has an average grain size of 71.4 μm with equiaxed grains. The analysis of thermal conductivity, thermal expansion, and TG-DSC experimental results showed that the cast WMoTaNb RHEA exhibits excellent stability at high temperatures above 1400 °C. This finding experimentally explains previous studies on phase and microstructural stability, providing experimental evidence for high stability and helping to explain the high-temperature mechanical behavior of the cast WMoTaNb RHEA at elevated temperatures.

Linjing Wang [109] et al. investigated the temporal evolution of coherent nanoscale precipitates in the $\text{Al}_{0.5}\text{Cr}_{0.9}\text{FeNi}_{2.5}\text{V}_{0.2}$ high-entropy alloy (HEA) during isothermal aging. When annealed at 600 °C for over 100 h, the nanoscale precipitates remained morphologically and distributionally stable, with no significant changes observed. This exceptional stability is primarily attributed to the lamellar nanostructure (Figure 16a–e), which imposes constraints on interface migration and long-range diffusion. Specifically, the Cr-rich nanoscale lamellar BCC phase partitions the Cr-depleted FCC ($L1_2$) matrix, creating barriers to diffusion and resulting in a kinetically sluggish coarsening rate. However, when the aging temperature was elevated to 700 °C, the lamellar BCC phase underwent spheroidization, disrupting the diffusion barriers and triggering significant coarsening. This phenomenon further validates the critical role of the nanoscale lamellar BCC phase in governing microstructural stability. These findings establish a design paradigm for alloys stabilized by lamellar nanostructures, achieving a favorable strength-ductility synergy alongside outstanding thermal stability.

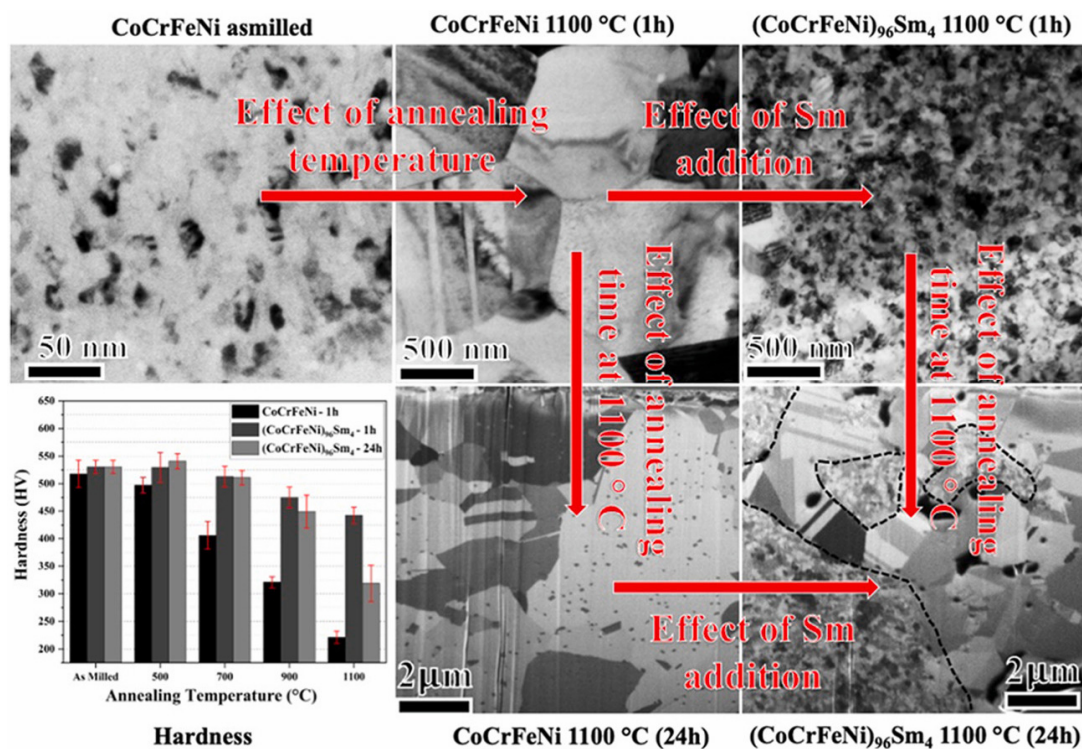


Figure 15. Microstructure and hardness evolution of CoCrFeNi-based with and without Sm addition under various annealing temperatures and durations [108].

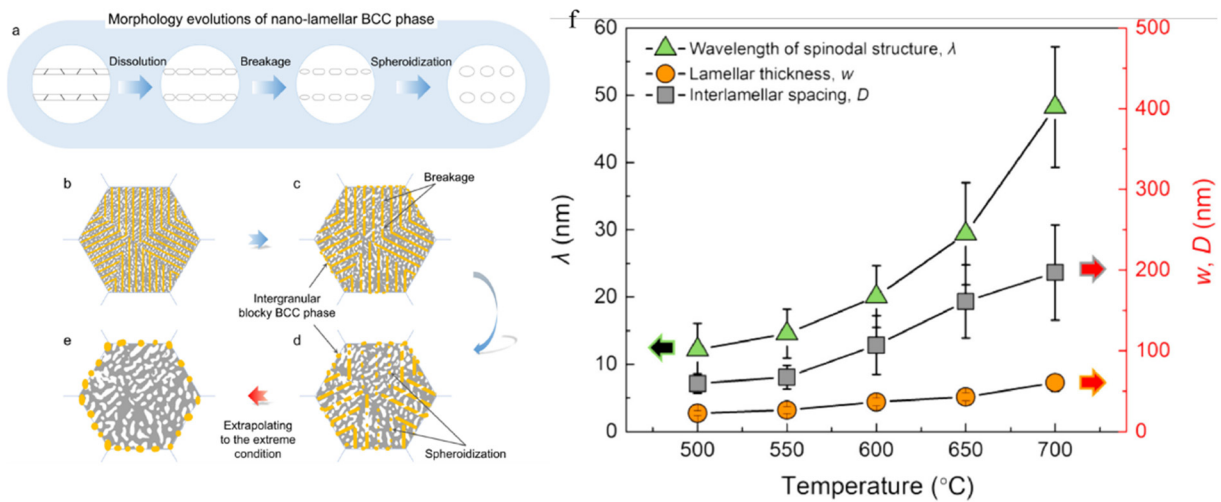


Figure 16. Schematic diagram for (a) morphology evolutions of lamellar precipitations, (b–d) morphology evolution precipitates with elevated aging temperature, and (e) microstructure of precipitates in alloy extrapolating to extreme conditions. (f) Lamellar thickness w and interlamellar spacing D of nano-lamellar BCC phase, and wavelength λ of spinodal structure (SDS) and aging temperature [109].

Cheenepalli Nagarjuna [110] developed a novel equiatomic CrFeNiTiV high-entropy alloy (HEA) through mechanical alloying (MA) and spark plasma sintering (SPS). Additionally, the effects of heat treatment temperature on the phase composition, microstructure, and mechanical properties of the HEA were investigated. The results showed that after 30 h of MA, a single body-centered cubic (BCC) phase was formed. Following SPS, the single-phase structure separated into BCC, Ni₃Ti, and TiC-rich phases, attributed to the large atomic radius difference and high mixing enthalpy of Ti with the other elements. Compared to sintered HEA, no change in the initial phase was observed after high-temperature heat treatment, though phase coarsening was noted. Microstructural analysis confirmed that after heat treatment at 1000 °C, the phases were uniformly distributed, and the interfaces were well bonded.

Wenjie Chen [111] conducted a computational study to investigate the effects of pressure and temperature on the phase stability and thermodynamic properties of the NbMoZrTiV LRHEA. Additionally, the microstructure and mechanical properties after annealing at different temperatures (600 °C, 800 °C, and 1000 °C) were examined. Both simulations and experimental results indicate that the NbMoZrTiV LRHEA exists as a single-phase BCC solid solution, with all crystal structures satisfying thermodynamic stability and showing no phase transformation with increasing pressure or temperature. As evidenced by the IPF and PF images in Figure 17, both the as-cast and annealed alloys exhibit random grain orientations without any noticeable texture. Notably, the grain size remains essentially unchanged as the annealing temperature increases, demonstrating the alloy’s excellent high-temperature phase stability.

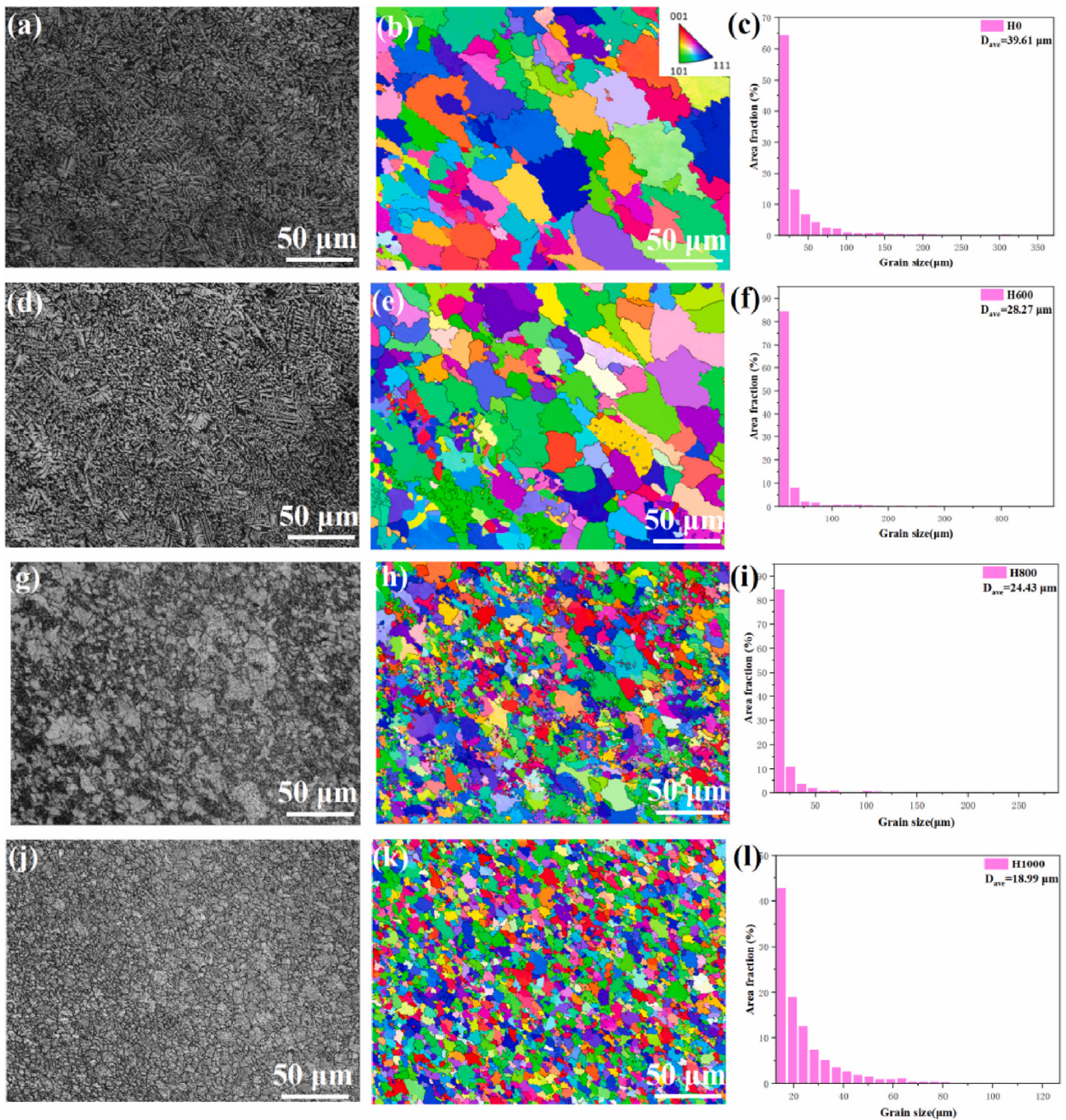


Figure 17. EBSD maps, IPF maps and grain size results for the NbMoZrTiV LRHEAs. (a–c) H0. (d–f) H600. (g–i) H800. (j–l) H1000 [111].

5. Conclusions and Prospects

HEAs exhibit exceptional multiple properties and hold broad application prospects, especially since some HEAs demonstrate excellent mechanical performance at elevated temperatures, making them promising candidates for high-temperature applications. This review summarizes the latest advances in the high-temperature, short-term mechanical properties, creep behavior, oxidation resistance, and phase stability of HEAs.

HEAs have demonstrated remarkable high-temperature mechanical properties owing to their unique multi-principal element design and tunable microstructures. Recent research has revealed that strengthening mechanisms such as solid-solution strengthening, $L1_2$ precipitate reinforcement, grain boundary engineering, and severe lattice distortion can be effectively combined to enhance both strength and ductility at elevated temperatures. Novel alloy systems—including $L1_2$ -strengthened Co-rich HEAs, B2/FCC eutectic systems, and refractory BCC-based HEAs—exhibit superior performance over wide temperature ranges, often surpassing traditional superalloys. Advanced processing techniques such as directional solidification, additive manufacturing, and tailored elemental partitioning further enable precise control of phase distribution and defect structures. These findings underscore the broad application potential of

HEAs in extreme thermal environments and provide critical insights into the future design of next-generation high-temperature structural materials.

The high-temperature creep resistance of HEAs stems from a combination of mechanisms, including solid solution strengthening, precipitation hardening, dislocation entanglement, and grain boundary stabilization. Tailoring alloy design based on dominant creep mechanisms offers strategic routes to optimization. Future work should emphasize the dynamic evolution of microstructure and transitions in deformation mechanisms under variable temperature-stress conditions for reliable application in extreme environments.

HEAs exhibit promising high-temperature oxidation resistance due to their unique elemental composition, complex microstructures, and sluggish diffusion effects. These studies underscore that optimizing oxidation resistance in HEAs requires integrated strategies involving selective oxidation, multi-phase synergy, and kinetic control. Protective oxide scales such as Al_2O_3 , Cr_2O_3 , and complex oxides like CrTaO_4 and AlNbO_4 can form in many HEAs, acting as effective diffusion barriers and ensuring long-term stability. The addition of elements such as Cr, Al, Si, and optimal Ti content significantly enhances oxidation resistance by promoting the formation of slow-growing, adherent oxide films. Conversely, excessive reactive elements (e.g., Hf, V) may destabilize the oxide scale or introduce volatile oxides. Microstructure refinement techniques, such as electron beam freeform fabrication (EBF³), contribute to improved oxidation performance by reducing grain boundary defects and forming multilayer oxide barriers. Studies also reveal that tailored alloy design—such as Y-Hf co-doping, Cr-rich compositions, and phase-optimized eutectic structures—further stabilizes the oxide/metal interface under cyclic or long-term conditions up to 1200 °C. These insights offer valuable guidance for the future development of HEAs with superior oxidation resistance for use in extreme thermal environments.

Phase stability is a cornerstone for ensuring the long-term reliability of HEAs under high-temperature service conditions. While conventional alloys often suffer from severe microstructural coarsening and phase decomposition at elevated temperatures, HEAs have demonstrated remarkable structural and compositional stability due to their sluggish diffusion kinetics and entropy-driven thermodynamic behavior. Recent studies have shown that maintaining stability requires a multifaceted approach. Strategies such as grain boundary pinning via elemental segregation, precipitation strengthening through thermodynamically stable and coherent secondary phases, phase transformation control in metastable ordered structures, and compositional optimization to suppress deleterious phase formation have all proven effective. Furthermore, engineering lamellar or nanocrystalline microstructures, including coherent precipitate-matrix architectures and nanoscale BCC/FCC domains, can inhibit interface migration and delay coarsening, thus preserving mechanical integrity even after prolonged thermal exposure. Experimental evidence, ranging from resistance to recrystallization and hardness degradation to creep and oxidation resistance, substantiates the feasibility of these mechanisms. Altogether, these findings establish a robust foundation for designing next-generation HEAs with superior phase and microstructural stability tailored for extreme thermal environments such as aerospace, nuclear, and high-efficiency energy systems.

Although considerable progress has been achieved in understanding the high-temperature performance of HEAs, several areas warrant further investigation:

1. **Composition-Microstructure-Property Relationships.** A deeper understanding of the interactions among multi-principal element compositions, microstructural evolution, and high-temperature performance is needed. Advanced characterization techniques (such as *in-situ* TEM and APT) combined with computational methods (like DFT and CALPHAD) should be employed to elucidate the atomic-scale deformation mechanisms and interactions.
2. **Long-term Stability under Cyclic Loading.** Most studies have focused on short-term performance, while the long-term stability under cyclic thermal and mechanical loads remains underexplored. Systematic evaluation of fatigue behavior, creep-fatigue interactions, and environmental degradation (for example, in corrosive atmospheres) is crucial for practical applications.
3. **Multi-Objective Optimization of High-Temperature Properties.** While high-temperature strength is an important aspect, other properties such as ductility, oxidation resistance, phase stability, and interfacial stability are also critical for structural materials at elevated temperatures. Currently, it is difficult for HEAs to meet all these performance criteria simultaneously. Therefore, optimizing the comprehensive high-temperature performance of HEAs through alloying strategies, process optimization, and other approaches is a key future research direction.
4. **Accelerated Discovery through Computational Tools and New Methods.** Given that HEAs comprise multiple principal elements and offer a vast compositional design space, machine learning, computational modeling, and high-throughput experiments can accelerate the discovery of new HEA compositions with tailored properties.

Author Contributions

Conceptualization, W.P., P.L.; Investigation, W.P., D.H., G.D.; Writing—Original Draft Preparation, W.P.; Writing—Review & Editing, P.L. Supervision, W.W.; Funding, P.L.

Ethics Statement

Not applicable.

Informed Consent Statement

Not applicable.

Data Availability Statement

Not applicable.

Funding

This work was financially supported by the Natural Science Foundation of Hunan Province (No. 2023JJ40737), National Natural Science Foundation of China (No. 52304361, No. 52130408).

Declaration of Competing Interest

The authors declare no competing financial interest.

References

1. Song W, Yang J, Liang J, Lu N, Zhou Y, Sun X, et al. A new approach to design advanced superalloys for additive manufacturing. *Addit. Manuf.* **2024**, *84*, 104098.
2. Bochenek K, Basista M. Advances in processing of NiAl intermetallic alloys and composites for high temperature aerospace applications. *Prog. Aerosp. Sci.* **2015**, *79*, 136–146.
3. George EP, Raabe D, Ritchie RO. High-entropy alloys. *Nat. Rev. Mater.* **2019**, *4*, 515–534.
4. Gong P, Liu XG, Rijkenberg A, Rainforth WM. The effect of molybdenum on interphase precipitation and microstructures in microalloyed steels containing titanium and vanadium. *Acta Mater.* **2018**, *161*, 374–387.
5. Fu W, Yang H, Li T, Sun J, Guo S, Fang D, et al. Enhancing corrosion resistance of ZK60 magnesium alloys via Ca microalloying: The impact of nanoscale precipitates. *J. Magnes. Alloys* **2023**, *11*, 3214–3230.
6. Zheng Q, Zhang L, Jiang H, Zhao J, He J. Effect mechanisms of micro-alloying element La on microstructure and mechanical properties of hypoeutectic Al-Si alloys. *J. Mater. Sci. Technol.* **2020**, *47*, 142–151.
7. Ajay P, Dabhade VV. Heat treatments of Inconel 718 nickel-based superalloy: A Review. *Met. Mater. Int.* **2024**, *31*, 1204–1231.
8. Makineni SK, Singh MP, Chattopadhyay K. Low-Density, High-Temperature Co Base Superalloys. *Annu. Rev. Mater. Res.* **2021**, *51*, 187–208.
9. Yan J, Gu Y, Li H, Yang F, Yuan Y, Zhang P, et al. Impact of Aging Temperature on the Performance of a Nickel-Iron-Based Superalloy. *Metall. Mater. Trans. A* **2018**, *49*, 1561–1570.
10. Zhang Q, Chang Y, Gu L, Luo Y, Ge B. Study of microstructure of nickel-based superalloys at high temperatures. *Scr. Mater.* **2017**, *126*, 55–57.
11. Shahwaz M, Nath P, Sen I. A critical review on the microstructure and mechanical properties correlation of additively manufactured nickel-based superalloys. *J. Alloys Compd.* **2022**, *907*, 164530.
12. Praveen S, Kim HS. High-Entropy Alloys: Potential Candidates for High-Temperature Applications—An Overview. *Adv. Eng. Mater.* **2018**, *20*, 1700645.
13. Dewangan SK, Mangish A, Kumar S, Sharma A, Ahn B, Kumar V. A review on High-Temperature Applicability: A milestone for high entropy alloys. *Eng. Sci. Technol.-Int. J.-Jestech* **2022**, *35*, 101211.
14. Wang Z, Chen S, Yang S, Luo Q, Jin Y, Xie W, et al. Light-weight refractory high-entropy alloys: A comprehensive review. *J. Mater. Sci. Technol.* **2023**, *151*, 41–65.
15. Sharma AS, Yadav S, Biswas K, Basu B. High-entropy alloys and metallic nanocomposites: Processing challenges, microstructure development and property enhancement. *Mater. Sci. Eng. R Rep.* **2018**, *131*, 1–42.
16. Zhang W-T, Wang X-Q, Zhang F-Q, Cui X-Y, Fan B-B, Guo J-M, et al. Frontiers in high entropy alloys and high entropy functional materials. *Rare Met.* **2024**, *43*, 4639–4776.
17. Miracle DB, Senkov ON. A critical review of high entropy alloys and related concepts. *Acta Mater.* **2017**, *122*, 448–511.

18. Tsai M-H, Yeh J-W. High-Entropy Alloys: A Critical Review. *Mater. Res. Lett.* **2014**, *2*, 107–123.
19. Nene SS, Sinha S, Yadav DK, Dutta A. Metallurgical aspects of high entropy alloys. *J. Alloys Compd.* **2024**, *1005*, 175849.
20. George EP, Curtin WA, Tasan CC. High entropy alloys: A focused review of mechanical properties and deformation mechanisms. *Acta Mater.* **2020**, *188*, 435–474.
21. Gao X, Lu Y, Zhang B, Liang N, Wu G, Sha G, et al. Microstructural origins of high strength and high ductility in an AlCoCrFeNi_{2.1} eutectic high-entropy alloy. *Acta Mater.* **2017**, *141*, 59–66.
22. Zhu B, Zhao D, Niu Y, Zhang Z, Zhao H. The short-range ordering and atomic segregation in various phases of high-entropy alloy during the solidification process. *Mater. Des.* **2023**, *234*, 112290.
23. Ren J, Wu M, Li C, Guan S, Dong J, Forien J-B, et al. Deformation mechanisms in an additively manufactured dual-phase eutectic high-entropy alloy. *Acta Mater.* **2023**, *257*, 119179.
24. Alvi S, Jarzabek DM, Kohan MG, Hedman D, Jenczyk P, Natile MM, et al. Synthesis and Mechanical Characterization of a CuMoTaWV High-Entropy Film by Magnetron Sputtering. *ACS Appl. Mater. Interfaces* **2020**, *12*, 21070–21079.
25. Alvi S, Milczarek M, Jarzabek DM, Hedman D, Kohan MG, Levintant-Zayonts N, et al. Enhanced Mechanical, Thermal and Electrical Properties of High-Entropy HfMoNbTaTiVWZr Thin Film Metallic Glass and its Nitrides. *Adv. Eng. Mater.* **2022**, *24*, 2101626.
26. Chen J, Zhou X, Wang W, Liu B, Lv Y, Yang W, et al. A review on fundamental of high entropy alloys with promising high-temperature properties. *J. Alloys Compd.* **2018**, *760*, 15–30.
27. Wang Y, Lin X, Zhao Y, Wang Z, Yu X, Gao X, et al. Laser powder bed fusion of Zr-modified Al-Cu-Mg alloy: Processability and elevated-temperature mechanical properties. *J. Mater. Sci. Technol.* **2023**, *136*, 223–235.
28. Wan Y, Cheng Y, Chen Y, Zhang Z, Liu Y, Gong H, et al. A Nitride-Reinforced NbMoTaWHfN Refractory High-Entropy Alloy with Potential Ultra-High-Temperature Engineering Applications. *Engineering* **2023**, *30*, 110–120.
29. Senkov ON, Miracle DB, Chaput KJ, Couzinie J-P. Development and exploration of refractory high entropy alloys—A review. *J. Mater. Res.* **2018**, *33*, 3092–3128.
30. Lim KR, Lee KS, Lee JS, Kim JY, Chang HJ, Na YS. Dual-phase high-entropy alloys for high-temperature structural applications. *J. Alloys Compd.* **2017**, *728*, 1235–1238.
31. Ye YF, Wang Q, Lu J, Liu CT, Yang Y. High-entropy alloy: challenges and prospects. *Mater. Today* **2016**, *19*, 349–362.
32. Su B, Zhu Y, Cheng F, Zhang Y, Li Z. Achieving exceptional high-temperature strength and oxidation resistance in an additively manufactured refractory high-entropy alloy via strategic elemental substitutions. *J. Alloys Compd.* **2025**, *1010*, 177079.
33. Wang P, Wu W, Pan A, Guo Z, Xia L, Cui F, et al. High temperature tensile properties and deformation behavior of CoCrFeNiW_{0.2} high entropy alloy. *Int. J. Refract. Met. Hard Mater.* **2024**, *124*, 106776.
34. Dai Q, Xie B, Yu Z, Zhu Z, Xu B, Sun M, et al. Tailoring the mechanical properties of a novel AlNbTi₃VZr_{1.5} refractory high-entropy alloy by controlling precipitates and B2 domains. *J. Alloys Compd.* **2025**, *1032*, 181094.
35. Guo R, Zhang P, Pan J, Xu J, Liu L, Zhang C, et al. Achieving prominent high-temperature mechanical properties in a dual-phase high-entropy alloy: A synergy of deformation-induced twinning and martensite transformation. *Acta Mater.* **2024**, *264*, 119591.
36. Wu Y, Brechtel J, Li C, Liaw PK, Geng G, Zhang Y. Serration behavior and brittle phase-induced mechanical transitions in wrought Al_{0.3}CoCrFeNi high-entropy alloy from 100 °C to 800 °C. *Mater. Sci. Eng. A* **2025**, *932*, 148261.
37. Tian Y, Wang B, Wei D, Kong D, Wang R, Zhu G, et al. Promoted room-temperature deformability and high-temperature strength synergy through zig-zag faceted interface design in TiNbTaWC_{0.7} eutectic refractory high-entropy alloy. *J. Mater. Res. Technol.* **2024**, *33*, 9507–9518.
38. Wan Y, Liang X, Cheng Y, Liu Y, He P, Zhang Z, et al. Superior high-temperature strength in a dual-BCC-phase NbMoTaWHf refractory high-entropy alloy. *Intermetallics* **2024**, *175*, 108515.
39. Wang Q, Yang W, Lin S, Liu C, Qin J, Qu P, et al. A novel L12-strengthened single crystal high entropy alloy with excellent high-temperature mechanical properties. *Mater. Charact.* **2024**, *212*, 113958.
40. Lv P, Liu L, Zhao G, Guo S, Zhou Z, Zhao Y, et al. Temperature effects on tensile behaviors and relevant deformation mechanisms of a low-cost nickel-based single crystal superalloy containing 1.5% Re. *J. Alloys Compd.* **2022**, *926*, 166819.
41. Shi L, Yu JJ, Cui CY, Sun XF. Temperature dependence of deformation behavior in a Co–Al–W-base single crystal superalloy. *Mater. Sci. Eng. A* **2015**, *620*, 36–43.
42. Gao L, Wu Y, An N, Chen J, Liu X, Bai R, et al. Nanoscale L12 phase precipitation induced superb ambient and high temperature mechanical properties in Ni–Co–Cr–Al system high-entropy superalloys. *Mater. Sci. Eng. A* **2024**, *898*, 145995.
43. Cao BX, Kong HJ, Ding ZY, Wu SW, Luan JH, Jiao ZB, et al. A novel L12-strengthened multicomponent Co-rich high-entropy alloy with both high γ' -solvus temperature and superior high-temperature strength. *Scr. Mater.* **2021**, *199*, 113826.
44. Pandey P, Sawant AK, Nithin B, Peng Z, Makineni SK, Gault B, et al. On the effect of Re addition on microstructural evolution of a CoNi-based superalloy. *Acta Mater.* **2019**, *168*, 37–51.
45. Chen Y, Wang C, Ruan J, Yang S, Omori T, Kainuma R, et al. Development of low-density γ/γ' Co–Al–Ta-based superalloys with high solvus temperature. *Acta Mater.* **2020**, *188*, 652–664.

46. Lee C, Song G, Gao MC, Feng R, Chen P, Brechtel J, et al. Lattice distortion in a strong and ductile refractory high-entropy alloy. *Acta Mater.* **2018**, *160*, 158–172.
47. Zhang Y, Yu K, Qin B, Yang C, Ye S, Feng C, et al. Origins of strength stabilities at elevated temperatures in additively manufactured refractory high entropy alloy. *Mater. Sci. Eng. A* **2024**, *915*, 147225.
48. Jia Y, Wang Z, Wu Q, Wei Y, Bai X, Liu L, et al. Boron microalloying for high-temperature eutectic high-entropy alloys. *Acta Mater.* **2024**, *262*, 119427.
49. Wang T, Jiang W, Wang X, Jiang B, Wang Y, Wang X, et al. Enhanced mechanical properties of lightweight refractory high-entropy alloys at elevated temperatures via Si addition. *Mater. Charact.* **2024**, *218*, 114552.
50. Guo NN, Wang L, Luo LS, Li XZ, Chen RR, Su YQ, et al. Microstructure and mechanical properties of refractory high entropy (Mo_{0.5}NbHf_{0.5}ZrTi)BCC/M5Si₃ in-situ compound. *J. Alloys Compd.* **2016**, *660*, 197–203.
51. Liu Y, Zhang Y, Zhang H, Wang N, Chen X, Zhang H, et al. Microstructure and mechanical properties of refractory HfMo_{0.5}NbTiV_{0.5}Si₆ high-entropy composites. *J. Alloys Compd.* **2017**, *694*, 869–876.
52. Li L, Fang Q, Li J, Liu B, Liu Y, Liaw PK. Lattice-distortion dependent yield strength in high entropy alloys. *Mater. Sci. Eng. A* **2020**, *784*, 139323.
53. Li W, Wang G, Wu S, Liaw PK. Creep, fatigue, and fracture behavior of high-entropy alloys. *J. Mater. Res.* **2018**, *33*, 3011–3034.
54. Song C, Li G, Li G, Zhang G, Cai B. Tensile creep behavior and mechanism of CoCrFeMnNi high entropy alloy. *Micron* **2021**, *150*, 103144.
55. Zhang L, Dou Y, Bai B, Yu B, He X, Yang W. Research progress on creep resistance of high entropy alloys. *J. Alloys Compd.* **2025**, *1011*, 178280.
56. Shen X, Sun B, Xin S, Ding S, Shen T. Creep in a nanocrystalline VNbMoTaW refractory high-entropy alloy. *J. Mater. Sci. Technol.* **2024**, *187*, 221–229.
57. You ZY, Tang ZY, Chu FB, Zhao L, Zhang HW, Cao DD, et al. Elevated-temperature creep properties and deformation mechanisms of a non-equiatomic FeMnCoCrAl high-entropy alloy. *J. Mater. Res. Technol.* **2024**, *30*, 3822–3830.
58. Zhang X, Bai P, Wang F, Zhao H, Zhou X, Wang S, et al. Atomistic insight into the effects of W content on the creep behaviors of NbMoTaW high-entropy alloys. *J. Mater. Res. Technol.* **2025**, *36*, 3289–3297.
59. Kral P, Blum W, Dvorak J, Yurchenko N, Stepanov N, Zherebtsov S, Kuncicka L, Kvapilova M, Sklenicka V. Creep behavior of an AlTiVNbZr_{0.25} high entropy alloy at 1073 K. *Mater. Sci. Eng. A* **2020**, *783*, 139291.
60. Saito T, Ishida A, Yuyama M, Takata Y, Kawagishi K, Yeh A-C, et al. Tensile Creep Behavior of Single-Crystal High-Entropy Superalloy at Intermediate Temperature. *Crystals* **2020**, *11*, 28.
61. Feng J, Wang B, Zhang Y, Zhang P, Liu C, Ma X, et al. High-temperature creep mechanism of Ti-Ta-Nb-Mo-Zr refractory high-entropy alloys prepared by laser powder bed fusion technology. *Int. J. Plast.* **2024**, *181*, 104080.
62. Li Y, Chen W, Lu C, Li H, Zheng W, Ma Y, et al. Microstructural evolution mediated creep deformation mechanism for the AlCoCrFeNi_{2.1} eutectic high-entropy alloy under different testing conditions. *Mater. Sci. Eng. A* **2022**, *857*, 144100.
63. Tsao T-K, Yeh A-C, Kuo C-M, Kakehi K, Murakami H, Yeh J-W, et al. The High Temperature Tensile and Creep Behaviors of High Entropy Superalloy. *Sci. Rep.* **2017**, *7*, 12658.
64. Zhang M, George EP, Gibeling JC. Tensile creep properties of a CrMnFeCoNi high-entropy alloy. *Scr. Mater.* **2021**, *194*, 113633.
65. Dobeš F, Hadraba H, Chlup Z, Dlouhý A, Vilémová M, Matějčíček J. Compressive creep behavior of an oxide-dispersion-strengthened CoCrFeMnNi high-entropy alloy. *Mater. Sci. Eng. A* **2018**, *732*, 99–104.
66. Cao CM, Xu J, Tong W, Hao YX, Gu P, Peng LM. Creep behaviour and microstructural evolution of Al_xCrMnFeCoNi high-entropy alloys. *Mater. Sci. Technol.* **2019**, *35*, 1283–1290.
67. Liu C-J, Gadelmeier C, Lu S-L, Yeh J-W, Yen H-W, Gorsse S, et al. Tensile creep behavior of HfNbTaTiZr refractory high entropy alloy at elevated temperatures. *Acta Mater.* **2022**, *237*, 118188.
68. Yang L, Sen S, Schliephake D, Vikram RJ, Laube S, Pramanik A, et al. Creep behavior of a precipitation-strengthened A2-B2 refractory high entropy alloy. *Acta Mater.* **2025**, *288*, 120827.
69. Gadelmeier C, Yang Y, Glatzel U, George EP. Creep strength of refractory high-entropy alloy TiZrHfNbTa and comparison with Ni-base superalloy CMSX-4. *Cell Rep. Phys. Sci.* **2022**, *3*, 100991.
70. Dai J, Zhu J, Chen C, Weng F. High temperature oxidation behavior and research status of modifications on improving high temperature oxidation resistance of titanium alloys and titanium aluminides: A review. *J. Alloys Compd.* **2016**, *685*, 784–798.
71. Liu CM, Wang HM, Zhang SQ, Tang HB, Zhang AL. Microstructure and oxidation behavior of new refractory high entropy alloys. *J. Alloys Compd.* **2014**, *583*, 162–169.
72. Yao D, Zhou C, Yang J, Chen H. Experimental studies and modeling of the oxidation of multiphase niobium-base alloys. *Corros. Sci.* **2009**, *51*, 2619–2627.
73. Arshad M, Bano S, Amer M, Janik V, Hayat Q, Bai M. High-Temperature Oxidation and Phase Stability of AlCrCoFeNi High Entropy Alloy: Insights from In Situ HT-XRD and Thermodynamic Calculations. *Materials* **2024**, *17*, 3579.

74. Zhang J, Wang C, Xie D, Li X, Chen H, Huang M, et al. High-Temperature Oxidation Behavior of the FeCoNiCr_{0.8}Al_{0.2} High-Entropy Alloy in Air. *J. Mater. Eng. Perform.* **2025**. <https://doi.org/10.1007/s11665-025-10924-0>
75. Xu Q, Wang J, Guo C, et al. Oxidation properties and microstructure evolution of oxidation layer for Cr_xNbMoTiV refractory high entropy alloys at elevated temperature. *J. Mater. Res. Technol.* **2025**, *36*, 5050–5062.
76. Wu Z, Yuwen P, Zhang Y, Zhou C. Microstructure and oxidation behavior of CoCrCuFeNi high entropy alloy at 900 °C. *J. Mater. Res. Technol.* **2025**, *36*, 7696–7704.
77. Peng J, Wang C, Lu D, Wang T, Lin O. High-temperature oxidation performance and corrosion resistance of laser clad MoNbVTa_{0.5}Si_x (x = 0,0.5) refractory high-entropy alloys. *Int. J. Refract. Met. Hard Mater.* **2025**, *130*, 107137.
78. Nagarjuna C, Lee H, Dewangan SK, Rao KR, Pillai GM, Kumar V, et al. Understanding the role of Si alloying on the structural, mechanical, wear and high temperature oxidation behavior of CrFeNiTiX (X=Si) high entropy alloys. *J. Mater. Res. Technol.* **2024**, *33*, 5119–5135.
79. Das A, Majumdar S. Observing the formation of oxide scale structures over novel TaMoNbCrAl_{0.5}Hf_{0.5} and TaMoNbCrAl refractory high entropy alloys during high-temperature oxidation. *Scr. Mater.* **2025**, *257*, 116484.
80. Hu H, Li F, Liu M, Yang D, Zhu Z, Shen Q, et al. High temperature oxidation behavior of the dual-phase AlCoCr_{0.5}Fe_{2.5}Ni_{2.5} and single phase Al_{0.25}CoCrFeNi high entropy alloys. *Intermetallics* **2025**, *176*, 108553.
81. Shao L, Jin X, Li H, Zhang W, Xu J, Wei W, et al. Synergistic enhancement of high-temperature oxidation resistance in lightweight AlFeCrMnTi high-entropy alloy via BCC phase and L21 nano-coherent precipitates. *Mater. Charact.* **2025**, *224*, 115033.
82. Naqvi RB, Khan MI, Hakeem A, Askar K, Bakhsh N. Investigating the High-Temperature Oxidation Behavior of (Ti_zrt_a)₅₀ni₂₅co₁₀cu₁₅ Equimolar Refractory High Entropy Alloy. *J. Mater. Res. Technol.* **2025**, *36*, 2690–2699.
83. Wei Y, Fu Y, Pan Z, Ma Y, Cheng H, Zhao Q, et al. Influencing factors and mechanism of high-temperature oxidation of high-entropy alloys: A review. *Int. J. Miner. Metall. Mater.* **2021**, *28*, 915–930.
84. Farraro RJ, McLellan RB. Diffusivity of oxygen and nitrogen in niobium. *Mater. Sci. Eng.* **1978**, *33*, 113–116.
85. Zhang J, Wu Q, Yang C, Yang Z, Yin B, Yang Y. Initial oxidation behavior of AlCrMoNbTi high-entropy alloys studied by DFT calculations and experiments. *Intermetallics* **2025**, *176*, 108549.
86. Liang M, Zhang J, Gao J, Yi H, Yin B, Yang Z, et al. Enhancing the oxidation resistance of AlCoCrNi high-entropy alloy via Ti-induced microstructural modifications. *Corros. Sci.* **2025**, *246*, 112746.
87. Li Z, Wang L, Yang Y, Liu C, Su B, Zhang Q, et al. High temperature oxidation behavior of TiNbMoAlSi refractory high entropy alloy developed by electron beam additive manufacturing. *J. Mater. Sci. Technol.* **2025**, *215*, 131–146.
88. Butler TM, Chaput KJ, Dietrich JR, Senkov ON. High temperature oxidation behaviors of equimolar NbTiZrV and NbTiZrCr refractory complex concentrated alloys (RCCAs). *J. Alloys Compd.* **2017**, *729*, 1004–1019.
89. Gorr B, Müller F, Azim M, Christ H-J, Müller T, Chen H, et al. High-Temperature Oxidation Behavior of Refractory High-Entropy Alloys: Effect of Alloy Composition. *Oxid. Met.* **2017**, *88*, 339–349.
90. Li Z, Wang L, Wang B, Li Z, Li Z, Zhang Y, et al. Oxidation behavior of Ti-Nb-Mo-Al-Six refractory high entropy alloy at 1000°C. *Corros. Sci.* **2022**, *206*, 110504.
91. Sheikh S, Bijaksana MK, Motallebzadeh A, Shafeie S, Lozinko A, Gan L, et al. Accelerated oxidation in ductile refractory high-entropy alloys. *Intermetallics* **2018**, *97*, 58–66.
92. Bauer P-P, Swadźba R, Klamann L, Laska N. Aluminum diffusion inhibiting properties of Ti₅Si₃ at 900 °C and its beneficial properties on Al-rich oxidation protective coatings on γ-TiAl. *Corros. Sci.* **2022**, *201*, 110265.
93. Li L, Chen Y, Huang A, Liu X, Zhang H, Zhang H, et al. A novel NiCoCrAlPt high-entropy alloy with superb oxidation resistance at 1200 °C. *Corros. Sci.* **2024**, *228*, 111819.
94. Guo M, Xu L, Zhao Y, Deng S, Li Z, Wei S. High temperature oxidation behavior and mechanism of MoNbVTa_{0.5}Crx refractory high entropy alloys. *Corros. Sci.* **2025**, *245*, 112672.
95. Schellert S, Gorr B, Laube S, Kauffmann A, Heilmaier M, Christ HJ. Oxidation mechanism of refractory high entropy alloys Ta-Mo-Cr-Ti-Al with varying Ta content. *Corros. Sci.* **2021**, *192*, 109861.
96. Robson JD. Modeling competitive continuous and discontinuous precipitation. *Acta Mater.* **2013**, *61*, 7781–7790.
97. Yeh J-W, Chen S-K, Lin S-J, Gan J-Y, Chin T-S, Shun T-T, et al. Nanostructured High-Entropy Alloys with Multiple Principal Elements: Novel Alloy Design Concepts and Outcomes. *Adv. Eng. Mater.* **2004**, *6*, 299–303.
98. Sikdar K, Bhattacharya A, Chottopadhyay C, Roy D, Mitra R. An insight into high temperature stability of microstructure and mechanical properties of bulk nanocrystalline (AlCoCrCuFeNi)₉₉B₁ high entropy alloy processed by mechanical alloying and spark plasma sintering. *Mater. Sci. Eng. A* **2025**, *936*, 148408.
99. Shah N, Rahul MR, Bysakh S, Phanikumar G. Microstructure stability during high temperature deformation of CoCrFeNiTa eutectic high entropy alloy through nano-scale precipitation. *Mater. Sci. Eng. A* **2021**, *824*, 141793.
100. Liu C, Li Y, Li J, Wang Z, Wang Q, Dong C, et al. A novel low-density and high-strength Fe-Ni-base high-entropy superalloy with stable γ/γ' coherent microstructure at 1023 K. *Scr. Mater.* **2024**, *252*, 116236.

101. Sharma A, Dasari S, Soni V, Kloenne Z, Couzinié J-P, Senkov ON, et al. B2 to ordered omega transformation during isothermal annealing of refractory high entropy alloys: Implications for high temperature phase stability. *J. Alloys Compd.* **2023**, *953*, 170065.
102. Fan A-C, Chen Y-S, Chi C-C, Miracle DB, Shiue J, Kuo P-C, et al. Stability of the B2 phase in Al-Nb-Ta-Ti-Zr refractory high-entropy superalloys: Resolving identification conflicts and offering practical solutions. *J. Alloys Compd.* **2025**, *1021*, 179591.
103. Yi H, Yin B, Yin F, Hu J, Liang M, Zhong W, et al. Clarifying the effects of composition and phase stabilization on the oxidation resistance in AlCoCrFeNiTi series high-entropy alloys at 1100 °C. *J. Alloys Compd.* **2025**, *1010*, 177087.
104. Whitfield TE, Pickering EJ, Owen LR, Senkov ON, Miracle DB, Stone HJ, et al. An assessment of the thermal stability of refractory high entropy superalloys. *J. Alloys Compd.* **2021**, *857*, 157583.
105. Mugale M, Garg M, Walunj G, Kandadai VAS, Jasthi BK, Borkar T. Tweaking AlNi atomic fraction to enhance the mechanical properties of low-density AlCuFeNiTi- based high entropy alloys. *J. Alloys Compd.* **2025**, *1024*, 180109.
106. Chen S, Tang Y, Zhang J, Yue X, Yang H, Tang H, et al. Low activation Ti30V30Cr5Zr5Ta30-XWX refractory high entropy alloys with excellent mechanical properties and phase stability. *Intermetallics* **2025**, *182*, 108780.
107. Sun J, Wu Z, Zhu Z, Nai MLS, An X. Enhanced thermal stability and mechanical properties of an additively manufactured CoCrNiFeMn high entropy alloy. *J. Mater. Sci. Technol.* **2025**, *237*, 115–127.
108. Kotan H, Koç RC, Batıbay AB. Remarkable thermal stability of nanocrystalline CoCrFeNi high entropy alloy achieved through the incorporation of rare-earth element samarium. *Intermetallics* **2025**, *178*, 108608.
109. Wang L, Xiao Y, Ren Y, et al. Hierarchical nanostructure stabilizing high content coherent nanoprecipitates in Al-Cr-Fe-Ni-V high-entropy alloy. *J. Mater. Sci. Technol.* **2024**, *200*, 61-68.
110. Nagarjuna C, Dewangan SK, Lee H, Ahn B. Evolution of phase stability and structural properties in CrFeNiTiV high-entropy alloy under high-temperature heat treatment conditions. *Mater. Sci. Eng. A* **2023**, *886*, 145680.
111. Chen W, Li X. Phase stability, microstructure and thermodynamic properties of NbMoZrTiV lightweight high-entropy refractory alloy. *J. Mater. Res. Technol.* **2025**, *34*, 2919–2934.